isvr Institute of Sound and Vibration Research

Structural Analysis of a Symmetric Structure Consisting of Two Beams and a Plate Based on a Wave Approach

Ji Woo Yoo, D.J. Thompson and N.S. Ferguson

ISVR Technical Memorandum 905

April 2003

University of Southampton

SCIENTIFIC PUBLICATIONS BY THE ISVR

Technical Reports are published to promote timely dissemination of research results by ISVR personnel. This medium permits more detailed presentation than is usually acceptable for scientific journals. Responsibility for both the content and any opinions expressed rests entirely with the author(s).

Technical Memoranda are produced to enable the early or preliminary release of information by ISVR personnel where such release is deemed to the appropriate. Information contained in these memoranda may be incomplete, or form part of a continuing programme; this should be borne in mind when using or quoting from these documents.

Contract Reports are produced to record the results of scientific work carried out for sponsors, under contract. The ISVR treats these reports as confidential to sponsors and does not make them available for general circulation. Individual sponsors may, however, authorize subsequent release of the material.

UNIVERSITY OF SOUTHAMPTON

INSTITUTE OF SOUND AND VIBRATION RESEARCH

DYNAMICS GROUP

Structural Analysis of a Symmetric Structure Consisting of Two Beams and a Plate Based on a Wave Approach

by

Ji Woo Yoo, D.J. Thompson and N.S. Ferguson

ISVR Technical Memorandum No: 905

April 2003

Authorised for issue by
Professor M.J. Brennan
Group Chairman

Contents

1. Introduction

In an earlier report [1], the dynamic characteristics of a coupled non-symmetric structure consisting of a beam and a plate were investigated using a wave approach. In this previous analysis, the propagating wavenumber of the coupled beam was calculated iteratively, and it was assumed that the nearfield wave in the coupled beam had the same wavenumber as the propagating wave. In this report, problems of convergence in the iteration method used for the wavenumber estimation at some frequencies are addressed by using Muller's method. Also, the nearfield wave is considered separately in the coupled beam and the corresponding plate wave response is then calculated for this case. The resulting coupled nearfield wavenumber displays differences from the travelling wavenumber originally determined.

As a step towards investigation of a framed structure such as four beams surrounding a plate, the previous analysis is then developed and extended for a structure consisting of two identical beams connected by a rectangular plate. By using symmetry, this structure can be assembled from solutions of a plate attached to one beam for which the opposite edge of the plate parallel to the beam is either pinned [1] or has a sliding condition. The synthesis procedure is described and some numerical results are shown.

Compared with the previous report, some boundary conditions have been changed. It is now assumed that the beam attached to the plate has infinite torsional stiffness. It seems reasonable that the ends of the beams in a framed structure will have sliding conditions rather than free conditions. Therefore, the sliding condition is considered in the present report. The approximate representation of the plate by a locally reacting impedance is maintained. Calculations are based on 400 frequency points covering the frequency band 10 Hz ~ 1 kHz, chosen to be logarithmically spaced.

First of all, the relationship between the coupled beam wavenumber and the plate wavenumber is presented. The relationship when the nearfield wave is considered in the beam

is also shown for the present case. The numerical analysis is then presented for a sliding boundary condition as well as a pinned condition for the non-symmetric structure consisting of a single beam and a plate. This is based on the separate travelling and nearfield wavenumbers of the beam and the numerical evaluation using Muller's method. Then a synthesis procedure is described for modelling a symmetric structure consisting of two beams and a plate using the combined response of the antisymmetric and symmetric behaviour of the non-symmetric structure, and numerical results are presented. Appendix A lists the nomenclature. In appendix B the influence of the iteration method on the result shown in [1] is reviewed. Muller's method is explained in detail and improved results due to its application are shown.

2. Infinite beam coupled to semi-infinite width plate

2.1 Travelling wavenumber of coupled beam

Figure 1 shows an infinite beam coupled on one side to a semi-infinite plate. In the previous report [1], the relationship between the travelling wavenumber of the infinite coupled beam and the plate wavenumber was derived and discussed. It was also previously assumed that the nearfield wavenumber of the beam is the same as the travelling wavenumber.

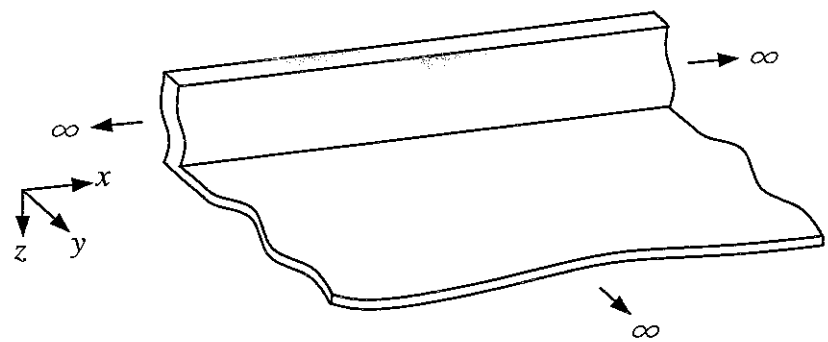

Figure 1. A built-up structure consisting of an infinite beam attached to a semi-infinite plate.

In this report, the nearfield wavenumber is considered separately and its relationship with the plate wavenumber is presented. Before mentioning the nearfield wavenumber, it seems appropriate to re-examine the relationship between the travelling wavenumber in an infinite coupled beam and that in the plate.

Previously [1], it was assumed that the beam had zero torsional stiffness. In this report, it is assumed instead that the beam is infinitely stiff to torsion along $y = 0$. This is because a beam which is infinitely stiff to torsion seems to be more similar to the physical behaviour of real structures consisting of several beams and plates, which will be considered in further studies.

Consider first the uncoupled free wave motion of the beam and plate. Harmonic motion at frequency ω is assumed throughout with a time dependence of $e^{i\omega t}$. The relevant equation of motion of the beam with no damping is [2]

$$D_b \frac{d^4 \tilde{w}_b}{dx^4} - m_b' \omega^2 \tilde{w}_b = 0 \qquad (2.1)$$

where $\tilde{w}_b$ is the complex amplitude of the beam vibration, D_b is the bending stiffness given by EI with E being the Young's modulus and I the second moment of area. m_b' is the mass per unit length.

A propagating harmonic flexural wave in the infinite beam, uncoupled from the plate, is given by

$$\tilde{w}_b = \tilde{A} e^{-ik_b x} \qquad (2.2)$$

where $\tilde{A}$ is the wave amplitude, x is the coordinate in the direction of propagation and k_b is the uncoupled beam wavenumber given by $k_b^4 = (m_b'/D_b)\omega^2$. Nearfield waves also exist with the form $e^{\pm k_b x}$.

The equation of motion of the plate with no damping is [3]

$$D_p\left(\frac{\partial^4\tilde{w}_p}{\partial x^4}+2\frac{\partial^4\tilde{w}_p}{\partial x^2\partial y^2}+\frac{\partial^4\tilde{w}_p}{\partial y^4}\right)-m_p''\omega^2\tilde{w}_p=0 \tag{2.3}$$

where $\tilde{w}_p$ is the complex amplitude of plate vibration, D_p is the plate bending stiffness given by $D_p=\frac{Eh^3}{12(1-\nu^2)}$, h is the plate thickness, ν is Poisson's ratio, and m_p'' is the mass per unit area of the plate. This leads to free wave solutions with wavenumber $k_p^4=m_p''\omega^2/D_p$.

When the semi-infinite plate and the infinite beam are joined along the line $y = 0$ a force per unit length $\tilde{F}(x)$ acts between them. Thus equation (2.1) becomes

$$D_b\frac{d^4\tilde{w}_b}{dx^4}-m_b'\omega^2\tilde{w}_b=-\tilde{F}(x) \tag{2.4}$$

Suppose that the free wave motion of the coupled beam becomes

$$\tilde{w}_b=\tilde{A}e^{-ik_x x} \tag{2.5}$$

for some wavenumber k_x. Then by trace wavenumber matching the motion of the plate is given by

$$\tilde{w}_P=(\tilde{B}e^{-ik_y y}+\tilde{C}e^{-k_e y})e^{-ik_x x} \tag{2.6}$$

where $\tilde{B}$ is the amplitude of the wave propagating away from the junction, $\tilde{C}$ is the amplitude of the near field wave in the plate which is also generated at the junction, k_y is the trace wavenumber for the propagating wave radiating into the plate normal to the beam and k_e is the trace wavenumber for the nearfield wave in the plate. In the above it is assumed that k_x is real, although as will be seen this is not quite the case.

To obtain the travelling wavenumber k_x in terms of the beam and plate properties, consider the propagating wave solution in the plate $\tilde{w}_p = \tilde{B}e^{-ik_y y}e^{-ik_x x}$. Substituting this into equation (2.3) gives

$$\{D_p(k_x^4 + 2k_y^2k_x^2 + k_y^4) - m_p''\omega^2\}\tilde{B}e^{-ik_y y}e^{-ik_x x} = 0. \tag{2.7}$$

As $\tilde{B}e^{-ik_y y}e^{-ik_x x} \neq 0$, the propagating normal trace wavenumber in the plate is found to be

$$k_y = \sqrt{k_p^2 - k_x^2}. \tag{2.8,a}$$

Similarly, let $\tilde{w}_p = \tilde{C}e^{-k_e y}e^{-ik_x x}$, then the normal near field wavenumber is

$$k_e = \sqrt{k_p^2 + k_x^2}. \tag{2.8,b}$$

The boundary conditions when a semi-infinite plate is attached at its edge to the beam are:

(i) Continuity equation; equal displacement

$$\tilde{w}_b(x) = \tilde{w}_p(x,0) \tag{2.9}$$

(ii) Sliding condition for the plate; the beam is assumed infinitely stiff to torsion along y=0

$$\left.\frac{\partial \tilde{w}_p}{\partial y}\right|_{y=0} = 0 \tag{2.10}$$

(iii) Force equilibrium condition; the force on the plate is equal and opposite to the force on the beam

$$D_p \frac{\partial}{\partial y}\left(\frac{\partial^2 \tilde{w}_p}{\partial y^2} + (2-\nu)\frac{\partial^2 \tilde{w}_p}{\partial x^2}\right)_{y=0} = \tilde{F}(x). \tag{2.11}$$

From the boundary condition (2.9),

$$\tilde{A} = \tilde{B} + \tilde{C}. \tag{2.12}$$

From the boundary condition (2.10),

$$\left[\left(-ik_y\tilde{B}e^{-ik_y y}-k_e\tilde{C}e^{-k_e y}\right)e^{-i\tilde{k}_e x}\right]_{y=0}=0. \tag{2.13}$$

$$\tilde{C}=-i\frac{k_y}{k_e}\tilde{B}.$$

$$\tilde{A}=\frac{k_e-ik_y}{k_e}\tilde{B}.$$

Therefore, the amplitudes of the waves in the plate are given by

$$\tilde{B}=\frac{k_e}{k_e-ik_y}\tilde{A},\quad \tilde{C}=\frac{-ik_y}{k_e-ik_y}\tilde{A}. \tag{2.14}$$

From the boundary condition (2.11),

$$D_p e^{-ik_x x}\left[ik_y\left\{k_y^2+(2-\nu)k_x^2\right\}\tilde{B}-k_e\left\{k_e^2-(2-\nu)k_x^2\right\}\tilde{C}\right]=\tilde{F}(x). \tag{2.15}$$

Substituting for $\tilde{B}$ and $\tilde{C}$ in terms of $\tilde{A}$ gives

$$\left[\frac{ik_y k_e\left\{k_y^2+k_e^2\right\}}{k_e-ik_y}\right]\tilde{A}D_p e^{-ik_x x}=\tilde{F}(x). \tag{2.16}$$

Therefore, the line impedance of the plate is

$$\tilde{Z}'_p=\frac{\tilde{F}(x)}{i\omega\tilde{A}e^{-ik_x x}}=\frac{D_p}{\omega}\left[\frac{k_y k_e 2k_p^2}{k_e-ik_y}\right]. \tag{2.17}$$

Finally, the general dispersion relationship for the built-up structure can be derived from equations (2.4) and (2.17).

$$D_b k_x^4=m'_b\omega^2-i\omega\,\tilde{Z}'_p. \tag{2.18}$$

There are two travelling wave solutions and two nearfield wave solutions to this equation. Note that k_x is not real, due to the damping-like term in $\tilde{Z}'_p$.

2.2 Nearfield wavenumber of coupled beam

A relationship can similarly be developed when the nearfield wavenumber in the beam is considered. Suppose that the nearfield wave motion of the beam is represented by

$$\tilde{w}_b = \tilde{A}' e^{-k_{nf}x}. \tag{2.19}$$

where k_{nf} is the nearfield wavenumber in the coupled beam.

Then the motion of the plate is given by

$$\tilde{w}_P = (\tilde{B}' e^{-ik'_y y} + \tilde{C}' e^{-k'_e y}) e^{-k_{nf}x} \tag{2.20}$$

where $\tilde{B}'$ is the amplitude of the travelling wave, $\tilde{C}'$ is the amplitude of the nearfield wave in the plate, k'_y is the trace wavenumber for the travelling wave radiating into the plate normal to the beam and k'_e is the trace wavenumber for the nearfield wave in the plate. The dash is used to distinguish them from the case when the travelling beam wavenumber is considered.

Now consider the travelling wave solution in the plate $\tilde{w}_p = \tilde{B}' e^{-ik'_y y} e^{-k_{nf}x}$ to obtain the nearfield wavenumber k_{nf}. Substituting this into equation (2.3) describing motion of the plate results in the following wavenumber relationship

$$\{D_p(k_{nf}^4 - 2k_y'^2 k_{nf}^2 + k_y'^4) - m_p'' \omega^2\} \tilde{B}' e^{-ik'_y y} e^{-k_{nf}x} = 0. \tag{2.21}$$

As $\tilde{B}' e^{-ik'_y y} e^{-k_{nf}x} \neq 0$, then $k_{nf}^4 - 2k_y'^2 k_{nf}^2 + k_y'^4 - k_p^4 = 0$. Therefore, the propagating normal trace wavenumber in the plate is

$$k'_y = \sqrt{k_p^2 + k_{nf}^2}. \tag{2.22,a}$$

Similarly, letting $\tilde{w}_p = \tilde{C}' e^{-k_e' y} e^{-k_{nf} x}$, then the nearfield wavenumber is

$$k_e' = \sqrt{k_p^2 - k_{nf}^2}. \qquad (2.22,b)$$

They are found by solving the dispersion equation similar to equation (2.18) using k_{nf} instead of k_x. These differ from the results k_y and k_e found for a travelling wave k_x in the beam.

The procedure to obtain the impedance when the beam nearfield wavenumber is considered is similar to the case when the travelling wavenumber is considered. All of the equations are the same except equation (2.15) the force equilibrium condition, which is

$$D_p e^{-k_{nf} x} \left[ik_y' \left\{ k_y'^2 - (2-\nu) k_{nf}^2 \right\} \tilde{B}' - k_e' \left\{ k_e'^2 + (2-\nu) k_{nf}^2 \right\} \tilde{C}' \right] = \tilde{F}(x). \qquad (2.23)$$

As k_{nf} terms are eliminated, the impedance equation is of the same form as equation (2.17).

2.3 Approximation by locally reacting impedance and general solution for the coupled structure

Note that if $k_p \gg k_x$ and $k_p \gg k_{nf}$ i.e. the plate wavenumber is much larger than the wavenumber in the coupled beam, then the exact line impedance of the plate, equation (2.17) can be written approximately as

$$\tilde{Z}_p' = \frac{\tilde{F}(x)}{i\omega \tilde{A} e^{-ik_x x}} \approx \frac{D_p k_p^3}{\omega}(1+i) = \frac{m_p'' \omega}{k_p}(1+i). \qquad (2.24)$$

Equation (2.24) is valid if the plate wavenumber is sufficiently larger than the coupled beam wavenumber, i.e., $k_x / k_p < 0.5$ [1]. Then the impedance of the plate can be considered as the input point impedance of an equivalent beam of infinite length and unit width driven by a point force.

3. Infinite beam coupled to finite width infinitely long plate

3.1 Travelling coupled wave for general boundary conditions on plate edge

The impedance of a finite width plate with a general boundary condition at the edge $y = L_y$, as shown in Figure 2, can be obtained from a wave approach. This structure is the same as that consisting of an infinite beam coupled to a finite width plate considered previously [1] apart from the revised boundary condition preventing rotation at $y = 0$.

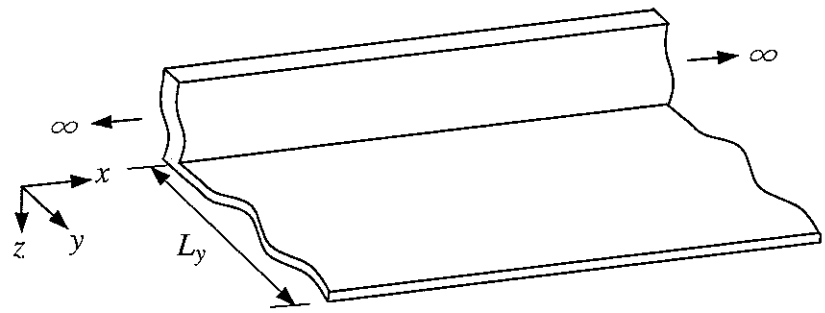

Figure 2. A built-up structure consisting of an infinite beam attached to a finite plate.

Assuming initially that there is no damping in the plate, the response in the infinitely long plate of width L_y joined to an infinitely long beam can be written as

$$\tilde{w}_P = (\tilde{B}e^{-ik_y y} + \tilde{C}e^{-k_e y} + \beta_y \tilde{r}\tilde{B}e^{ik_y y} + \tilde{D}e^{k_e(y-L_y)})e^{-ik_x x} \qquad (3.1)$$

where $\beta_y = e^{-ik_y 2L_y}$ represents a phase shift over length $2L_y$, $\tilde{r}$ is the complex reflection coefficient at the edge of the plate $y = L_y$ and $\tilde{D}$ is the amplitude of the nearfield wave which is generated at the opposite edge of the plate. The response of the beam is assumed to be $\tilde{w}_b = \tilde{A}e^{-ik_x x}$ as before.

The boundary conditions when a finite plate is attached at its edge to the beam are the same as for the semi-infinite plate structure.

Therefore, from the first boundary condition (2.9),

$$\tilde{A} = \tilde{B} + \tilde{C} + \beta_y \tilde{r} B + \tilde{D} e^{-k_e L_y}. \tag{3.2}$$

From the second boundary condition (2.10),

$$\left[\left(-ik_y \tilde{B} e^{-ik_y y} - k_e \tilde{C} e^{-k_e y} + ik_y \beta \tilde{r} \tilde{B} e^{ik_y y} + k_e \tilde{D} e^{k_e (y - L_y)} \right) e^{-i\tilde{k}_e x} \right]_{y=0} = 0. \tag{3.3}$$

Because the beam is attached to the edge $y = 0$ of the plate, at sufficiently high frequency it can be assumed that the influence of the nearfield from the opposite edge will be negligible, which means $\tilde{D} e^{-k_e L_y} \approx 0$. Therefore, the approximate amplitudes of the waves in the plate are given by

$$\tilde{C} = \frac{-ik_y (1 - \beta \tilde{r})}{k_e (1 + \beta \tilde{r}) - ik_y (1 - \beta \tilde{r})} \tilde{A}, \quad \tilde{B} = \frac{k_e}{k_e (1 + \beta \tilde{r}) - ik_y (1 - \beta \tilde{r})} \tilde{A}. \tag{3.4}$$

From the force equilibrium boundary condition (2.11),

$$D_p e^{-ik_x x} \left[ik_y \left\{ k_y^2 + (2 - \nu) k_x^2 \right\} (1 - \beta_y \tilde{r}) \tilde{B} - k_e \left\{ k_e^2 - (2 - \nu) k_x^2 \right\} \tilde{C} \right] = \tilde{F}(x). \tag{3.5}$$

Substituting for $\tilde{B}$ and $\tilde{C}$ in terms of $\tilde{A}$ and eliminating k_x gives

$$\left[\frac{ik_y k_e (1 - \beta_y \tilde{r}) \left\{ k_y^2 + k_e^2 \right\}}{k_e (1 + \beta_y \tilde{r}) - ik_y (1 - \beta_y \tilde{r})} \right] \tilde{A} D_p e^{-ik_x x} = \tilde{F}(x). \tag{3.6}$$

from which the line impedance of the plate, which is the impedance per unit length along the beam, is given by

$$\tilde{Z}'_p = \frac{\tilde{F}(x)}{i\omega \tilde{A} e^{-ik_x x}} = \frac{D_p}{\omega} \left[\frac{k_y k_e (1 - \beta_y \tilde{r}) 2k_p^2}{k_e (1 + \beta_y \tilde{r}) - ik_y (1 - \beta_y \tilde{r})} \right] \tag{3.7}$$

3.2 Nearfield coupled wave for general boundary conditions on plate edge

Now consider the nearfield wave in the coupled beam. In this case, equation (3.2) and (3.3) are not changed apart from changing k_y to k_y' and k_e to k_e', but equation (3.5) will be changed into

$$D_p e^{-k_{nf}x}\left[ik_y'\left\{k_y'^2-(2-\nu)k_{nf}^2\right\}(1-\beta_y\tilde{r})\tilde{B}'-k_e'\left\{k_e'^2+(2-\nu)k_{nf}^2\right\}\tilde{C}'\right]=\tilde{F}(x). \quad (3.8)$$

Once k_{nf} has been eliminated from this equation, the equation for the impedance is the same as equation (3.7). Note that even though the equation is not changed, a different value will be calculated because the impedance includes k_y', k_e' and the phase shift β_y which is a function of k_y', all of which differ from the values applying to a travelling wave k_x.

3.3 Approximate impedance and inclusion of the plate damping

The relationship between the wavenumbers k_p, k_y, k_e, k_x and k_{nf} is the same as for the semi-infinite plate structure of the previous section but should be found iteratively from the dispersion equation similar to equation (2.18). If the plate wavenumber greatly exceeds the beam wavenumber i.e. $k_p >> k_x$, then $\tilde{k}_y \approx \tilde{k}_p$, $\tilde{k}_e \approx \tilde{k}_p$, $\tilde{k}_y^2+\tilde{k}_e^2 \approx 2\tilde{k}_p^2$, and the line impedance of the plate equation (3.7) can be expressed in the simpler form

$$\tilde{Z}_p' \approx \frac{D_p 2k_p^3}{\omega}\left(\frac{1-\beta_y\tilde{r}}{(1+\beta_y\tilde{r})-i(1-\beta_y\tilde{r})}\right). \quad (3.9)$$

where $\tilde{r}$ depends on the reflection boundary conditions at $y=L_y$. For a pinned condition, the reflection coefficient $\tilde{r}$ becomes -1 while for a sliding condition $\tilde{r}=+1$. $\tilde{Z}_p'$ in equation (3.9) can be considered as like a locally reacting impedance as in section 2.3. Although equation (3.9) no longer contains k_y, k_e etc., explicitly, however, the factor β_y

still retains a dependence on k_y. It is therefore not a completely locally reacting impedance. Nevertheless, it can still be considered as a good approximation of the impedance of the plate.

If hysteretic damping is introduced into the plate, the plate stiffness is described as $\tilde{D}_p = D_p(1+i\eta_p)$ and the wavenumber of the damped plate becomes $\tilde{k}_p \approx k_p(1-i\eta_p/4)$ assuming $\eta_p \ll 1$. Now, equation (3.9) can be modified as follows to include damping terms.

$$\tilde{Z}'_p = \frac{\tilde{F}(x)}{i\omega\tilde{A}e^{-ik_x x}} \approx \frac{\tilde{D}_p 2\tilde{k}_p^3}{\omega}\left(\frac{1-\tilde{\beta}_y\tilde{r}}{(1+\tilde{\beta}_y\tilde{r})-i(1-\tilde{\beta}_y\tilde{r})}\right). \tag{3.10}$$

where $\tilde{\beta}_y = e^{-i\tilde{k}_y 2L_y}$ is the propagating wave attenuation coefficient of the plate, which represents attenuation as well as phase shift over the distance $2L_y$, i.e. twice the plate width.

3.4 Solution for coupled wavenumber

The general dispersion relationship for the infinite beam attached to the finite plate can be derived from equations (2.4) and (3.10), and has the same form as equation (2.18).

$$D_b k_x^4 = m'_b\omega^2 - i\omega\,\tilde{Z}'_p. \tag{3.11}$$

If $\tilde{Z}'_p = 0$, which means the beam becomes uncoupled from the plate, then equation (3.11) has four roots $\tilde{k}_x$ (actually k_b). However, because the impedance term $\tilde{Z}'_p$ which includes $\tilde{\beta}_y = e^{-i\tilde{k}_y 2L_y}$ depends on $\tilde{k}_x$, the equation becomes more complicated and it might be possible that there are more than four roots. Nevertheless, concerning the present case when the plate is flexible compared with the beam, there are only two propagating wave solutions (k_x) and two nearfield wave solutions (k_{nf}) to equation (3.11) that are close to k_b, the corresponding solutions for $\tilde{Z}'_p = 0$. Note that k_x is not real, due to the impedance term $\tilde{Z}'_p$. Each case must be solved from the corresponding impedance and should be solved

iteratively as k_x is contained in $\tilde{Z}'_p$. At some specific frequencies, for example when k_x becomes large and accordingly k_y becomes small, k_x does not converge using a simple iteration method. In this case, k_x can be calculated using Muller's method (see Appendix B for the use of Muller's method for the estimation of coupled wavenumbers).

4. Finite beam coupled to finite rectangular plate

4.1 Beam response for the coupled system

To derive the dispersion relationships for a coupled beam and plate, an infinite beam and a plate of finite width were used in the previous section. This general relationship can be extended to the structure which is finite in length as shown in Figure 3, where it is assumed that the beam has a sliding boundary at both ends.

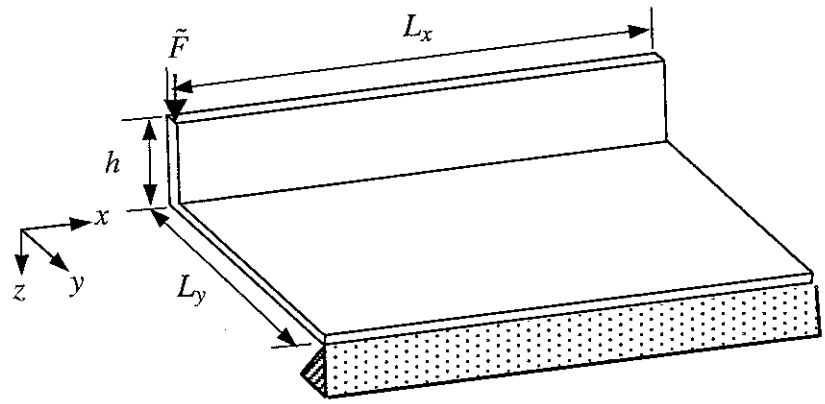

Figure 3. A built-up structure consisting of a finite beam attached to a finite plate with a pinned opposite edge.

It is thought that for a completely framed plate which might be considered later, the ends of the beam at the corners will be very stiff points and mainly able to displace but not rotate. This is due to the high (infinite) torsional stiffness applied by the perpendicular beams.

The general solution for the motion of the uncoupled finite beam at frequency ω is

$$\tilde{w} = \tilde{A}_1 e^{-i\tilde{k}_b x} + \tilde{A}_2 e^{-\tilde{k}_b x} + \tilde{A}_3 e^{i\tilde{k}_b x} + \tilde{A}_4 e^{\tilde{k}_b x} \tag{4.1}$$

where $\tilde{A}_1$ and $\tilde{A}_3$ are the amplitudes of travelling waves, $\tilde{A}_2$ and $\tilde{A}_4$ are the amplitudes of the nearfield waves, $\tilde{k}_b$ is the uncoupled travelling wavenumber of a damped beam. Now, if the plate is coupled to this beam, then it can be assumed that the solution for the motion of the finite beam possessing the coupled wavenumbers is

$$\tilde{w} = \tilde{A}_1 e^{-i\tilde{k}_x x} + \tilde{A}_2 e^{-\tilde{k}_{nf} x} + \tilde{A}_3 e^{i\tilde{k}_x x} + \tilde{A}_4 e^{\tilde{k}_{nf} x} \tag{4.2}$$

where $\tilde{A}_1$ and $\tilde{A}_3$ are the amplitudes of travelling waves, $\tilde{A}_2$ and $\tilde{A}_4$ are the amplitudes of the nearfield waves which have different values from those of equation (4.1), $\tilde{k}_x$ and $\tilde{k}_{nf}$ are the complex travelling wavenumber and nearfield wavenumber respectively, as determined in the previous section.

If the beam has length L_x with a force $\tilde{F}_0$ applied at one end x = 0, and has sliding boundary conditions at both ends, the boundary conditions are then given by

$$\tilde{D}_b \left.\frac{\partial \tilde{w}}{\partial x}\right|_{x=0} = 0, \tag{4.3a}$$

$$\tilde{D}_b \left.\frac{\partial^3 \tilde{w}}{\partial x^3}\right|_{x=0} = \tilde{F}_0, \tag{4.3b}$$

$$\tilde{D}_b \left.\frac{\partial \tilde{w}}{\partial x}\right|_{x=L_x} = 0, \tag{4.3c}$$

$$\tilde{D}_b \left.\frac{\partial^3 \tilde{w}}{\partial x^3}\right|_{x=L_x} = 0\,. \tag{4.3d}$$

Equations (4.3) can also be written in a matrix form,

$$\begin{bmatrix} -ik_x & -k_{nf} & ik_x & k_{nf} \\ ik_x^3 & -k_{nf}^3 & -ik_x^3 & k_{nf}^3 \\ -ik_x e^{-i\tilde{k}_x L_x} & -k_{nf} e^{-\tilde{k}_{nf} L_x} & ik_x e^{i\tilde{k}_x L_x} & k_{nf} e^{\tilde{k}_{nf} L_x} \\ ik_x^3 e^{-i\tilde{k}_x L_x} & -k_{nf}^3 e^{-\tilde{k}_{nf} L_x} & -ik_x^3 e^{i\tilde{k}_x L_x} & k_{nf}^3 e^{\tilde{k}_{nf} L_x} \end{bmatrix} \begin{Bmatrix} \tilde{A}_1 \\ \tilde{A}_2 \\ \tilde{A}_3 \\ \tilde{A}_4 \end{Bmatrix} = \begin{Bmatrix} 0 \\ \tilde{F}_0 / \tilde{D}_b \\ 0 \\ 0 \end{Bmatrix}. \tag{4.4}$$

Having solved this for the amplitudes $\tilde{A}_i$, the transfer mobility from the excitation point $x = 0$ to the response at an arbitrary position x can be calculated from the relationship between the force and velocity,

$$\tilde{Y}_{beam}(x) = \frac{i\omega\tilde{w}(x)}{\tilde{F}_0} = \frac{\omega}{\tilde{D}_b} \frac{\tilde{A}_1 e^{-i\tilde{k}_x x} + \tilde{A}_2 e^{-\tilde{k}_{nf} x} + \tilde{A}_3 e^{i\tilde{k}_x x} + \tilde{A}_4 e^{\tilde{k}_{nf} x}}{\tilde{k}_x^3 \tilde{A}_1 + i\tilde{k}_{nf}^3 \tilde{A}_2 - \tilde{k}_x^3 \tilde{A}_3 - i\tilde{k}_{nf}^3 \tilde{A}_4}. \tag{4.5}$$

4.2 Plate response for the coupled system

The response of the plate for a travelling wave in the beam is as given in equation (3.1), and by obtaining the coefficients in the equation, the response can be determined. The coefficients will be calculated from equations (2.9) ~ (2.11) which describe the boundary conditions. This process is carried out separately for each of the four waves in the beam.

Previously [1], the nearfield wavenumber in the coupled beam k_{nf} was assumed to be the same as the travelling wavenumber. In the present report, both wave types are considered and the plate response is calculated from consideration of each beam wave and the corresponding plate impedance separately. By adding the four different responses of the plate generated by the four different waves in the beam, which are a forward travelling wave ($kx+$), backward wave ($kx-$), forward nearfield wave ($knf+$) and backward nearfield wave ($knf-$), the plate response can be obtained. It has been assumed in adopting this approach that interaction between the beam and the plate can be treated separately for each wave in the beam.

Even if the four different beam waves are considered, the displacement continuity boundary condition (2.9) and the sliding boundary condition (2.10) can simply be applied using the corresponding wavenumbers. The force equilibrium condition (2.11), describing the force acting on the plate from the beam, is more complicated than the first two boundary conditions mentioned. If the plate can be represented in terms of a line impedance $\tilde{Z}'_p$, the force can be expressed in terms of the velocity and impedance

$$\tilde{F}(x) = \tilde{V}_{beam}(x)\tilde{Z}'_p = \tilde{F}_0 \tilde{Y}_{beam}(x)\tilde{Z}'_p \tag{4.6}$$

where $\tilde{F}_0$ is the force applied to the beam and $\tilde{Y}_{beam}(x)$ is the transfer mobility of the coupled beam, given by equation (4.5). Note that actually the approximation by the locally reacting impedance is used in equation (4.6) instead of the line impedance.

Although the impedance $\tilde{Z}'_p$ differs for a travelling or nearfield wave on the beam, the impedance for the travelling wave has the same value regardless of its propagation direction. The same is true for the nearfield wave. Therefore, equation (4.6) can be decomposed in terms of the different wave types as follows.

$$\tilde{F}_{kx+}(x) = \tilde{V}_{kx+}(x)\tilde{Z}'_{p,kx} \tag{4.7,a}$$

$$\tilde{F}_{kx-}(x) = \tilde{V}_{kx-}(x)\tilde{Z}'_{p,kx} \tag{4.7,b}$$

$$\tilde{F}_{knf+}(x) = \tilde{V}_{knf+}(x)\tilde{Z}'_{p,knf} \tag{4.7,c}$$

$$\tilde{F}_{knf-}(x) = \tilde{V}_{knf-}(x)\tilde{Z}'_{p,knf}\,. \tag{4.7,d}$$

Therefore, from the three boundary conditions at the attachment edge and those at the ends of the beam, the plate wave amplitude coefficients $\tilde{B}, \tilde{C}$, and $\tilde{D}$ can be obtained. In the

calculation of impedance and the plate response, it is assumed that $\tilde{D}e^{-k_e L_y} \approx 0$. Note that four different responses of the plate corresponding to equations (4.7a ~ d) will be obtained.

4.3 Power balance investigation

The total power input to the coupled structure and the power transferred to the plate were compared previously [1]. If the power dissipated in the beam and plate are determined, the power balance in the coupled structure can be considered. By conservation of energy, the total input power should be the same as the sum of the net power transferred to the plate and the power dissipated in the beam. Also the net power transferred to the plate should be the same as the power dissipated in the plate. These relationships are presented simply in Figure 4.

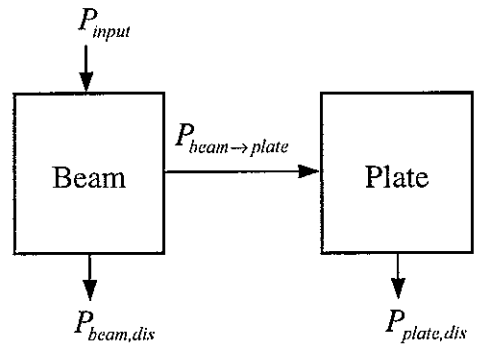

Figure 4. Power balance between subsystems of the coupled structure as in Figure 3.

The net power transferred from the beam to the plate can be simply expressed in terms of the force and response as follows.

$$P_{beam \rightarrow plate} = \frac{1}{2}\int_0^{L_x} \mathrm{Re}\left\{\tilde{F}^* \tilde{V}_{beam}\right\} dx, \qquad (4.8)$$

where $\tilde{F}$ is the force acting on the plate calculated from equation (4.6), $\tilde{V}_{beam}$ is the response of the coupled beam, L_x is the length of the beam and * indicates complex conjugate. This equation can be expanded as follows when the travelling and nearfield

wavenumber are separately considered.

$$P_{beam\to plate} = \frac{1}{2}\int_0^{L_x} \mathrm{Re}\left\{\left(\tilde{V}_{beam,kx}\tilde{Z}'_{p,kx} + \tilde{V}_{beam,knf}\tilde{Z}'_{p,knf}\right)^* \left(\tilde{V}_{beam,kx} + \tilde{V}_{beam,knf}\right)\right\} dx . \qquad (4.9)$$

Although the dissipated power in each subsystem can be obtained from either the kinetic or potential energy, because the beam structure does not have many vibrational modes in the frequency band of interest (less than 10 modes below 1 kHz in the present case), it is more appropriate to use the potential energy (strain energy). Strain energy can be calculated from the elasticity of the structure. Power is dissipated because structural damping is assumed by using a complex value for Young's modulus of elasticity. The maximum strain energy in a cycle in the beam is

$$E_{beam} = \frac{D_b}{2}\int_0^{L_x} \left|\frac{d^2\tilde{w}_b}{dx^2}\right|^2 dx , \qquad (4.10)$$

and the dissipated power in the beam can be written as [4]

$$P_{beam,dis} = \omega\eta_b E_{beam} . \qquad (4.11)$$

The strain energy of a plate is given by [2]

$$E_{plate,strain} = \frac{D_p}{2}\int_0^{L_x}\int_0^{L_y} \left[\left(\frac{\partial^2\tilde{w}_p}{\partial x^2}\right)^2 + \left(\frac{\partial^2\tilde{w}_p}{\partial y^2}\right)^2 + 2\nu\frac{\partial^2\tilde{w}_p}{\partial x^2}\frac{\partial^2\tilde{w}_p}{\partial y^2} + 2(1-\nu)\left(\frac{\partial^2\tilde{w}_p}{\partial x\partial y}\right)^2\right] dydx . \qquad (4.12)$$

However, in the present report the approximate plate impedance is assumed, which means that the plate can be thought of as many strips along the beam. Therefore, the dissipated energy in the plate can be represented as the sum of dissipated energy of each strip. The maximum strain energy of a strip in a cycle can therefore be expressed as

$$E_{strip} = \frac{D_p}{2}\int_0^{L_y} \left|\frac{\partial^2\tilde{w}_p}{\partial y^2}\right|^2 dy . \qquad (4.13)$$

Therefore, the strain energy for the whole area of the plate is

$$E_{plate} \simeq \int_0^{L_x} E_{strip} dx = \frac{D_p}{2} \int_0^{L_x} \int_0^{L_y} \left| \frac{\partial^2 \tilde{w}_p}{\partial y^2} \right|^2 dy dx, \tag{4.14}$$

and the dissipated power in the plate is

$$P_{plate,dis} = \omega \eta_p E_{plate}. \tag{4.15}$$

4.4 Numerical analysis - plate in pinned condition

In this section some numerical results are given for the built-up structure shown in Figure 3, the dimensions of which are given in Table 1. These dimensions are the same as those used in the previous report [1] except L_y which was previously 0.45 m. The second moment of area of the beam is calculated, as before, by assuming that its neutral axis lies in the mid-plane of the plate which is attached to the bottom of the beam.

Table 1. Dimensions of the built-up structure shown in Figure 3.

Material	Perspex	Plate width, L_y (m)	0.75
Young's modulus, E (GNm^{-2})	4.4	Thickness, t (mm)	5.9
Poisson's ratio, ν	0.38	Height of the beam, h (mm)	68.0
Density, ρ (kgm^{-3})	1152.0	Loss factor of the beam, η_b	0.05
Beam length, L_x (m)	2.0	Loss factor of the plate, η_p	0.05

The numerical analysis procedure is the same as before. Therefore, only some important results are mentioned and most physical phenomena are the same as those observed previously. Results are also compared with those obtained by a finite element analysis.

The edge parallel to the beam is considered as a pinned condition, which will be compared with the sliding condition in section 4.5 later.

4.4.1 Wavenumbers

Firstly, the various wavenumbers are compared for the damped plate in Figure 5 and Figure 6. Figure 5 shows the travelling wavenumber k_x in the coupled beam and the corresponding wavenumbers in the plate. Meanwhile, the nearfield wavenumber k_{nf} in the coupled beam and its corresponding wavenumber in the plate are shown in Figure 6. The uncoupled beam wavenumber, k_b is shown for comparison. It can be seen that the curves of k_p and k_b are exactly parallel as expected.

The coupled beam wavenumber k_x shows peaks and dips because of the impedance of the finite width plate attached to the beam. At the resonances of the plate the impedance $\tilde{Z}'_p$ is small and the wavenumber k_x is close to k_b. At the anti-resonances k_x is increased considerably (see Figure 9).

The asymptotic value of the coupled wavenumber k_x is higher than k_b. The reason can be seen from the dispersion equation which includes the impedance term of the plate. Its mass-like component increases k_x. Note that the slope of the asymptotic value of k_x is lower than that of k_b. This is because the equivalent mass in the impedance is reduced with increasing frequency.

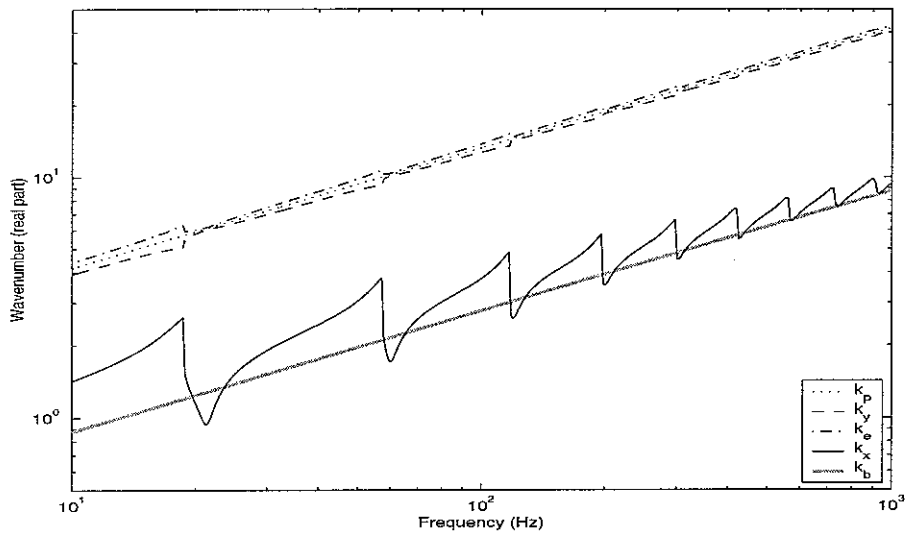

Figure 5. Comparison of the travelling wavenumber of the beam and the corresponding wavenumbers of the plate of the built-up structure as in Figure 3 (real part only, $\eta_p = 0.05$ in the plate, $\eta_b = 0.05$ in the beam).

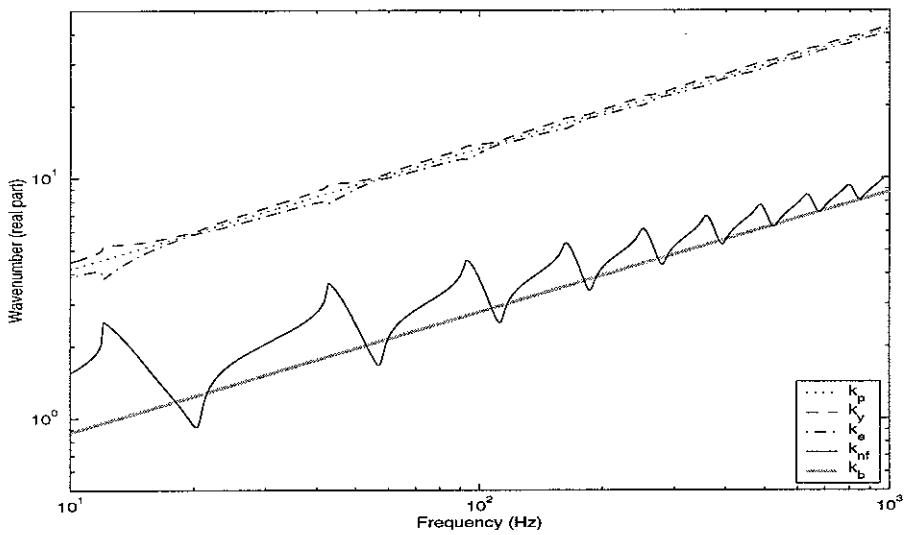

Figure 6. Comparison of the nearfield wavenumber of the beam and the corresponding wavenumbers of the plate of the built-up structure as in Figure 3 (real part only, $\eta_p = 0.05$ in the plate, $\eta_b = 0.05$ in the beam).

Comparing Figure 5 and 6, it can be seen how the plate wavenumbers are changed due to the travelling and nearfield wavenumbers of the beam, as was explained from equations (2.8)

and (2.22) in section 2. It can be seen that the travelling and nearfield waves of the plate can be approximated by the free wavenumber of the plate in both cases.

In Figure 7, a comparison is given of the imaginary parts of the travelling wavenumber and nearfield wavenumber in the coupled beam as well as the corresponding real parts.

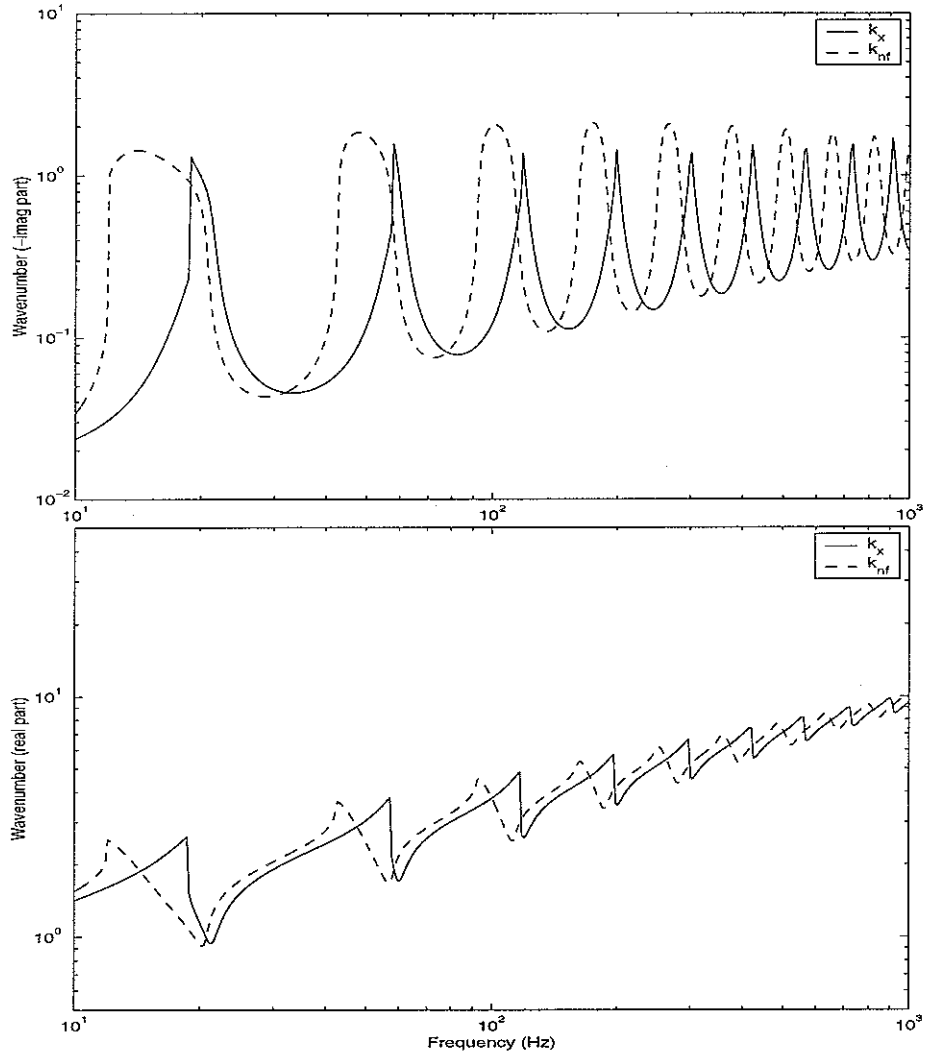

Figure 7. Comparison of the beam travelling and the nearfield wavenumber in the built-up structure consisting of the finite beam and the finite plate as in Figure 3 ($\eta_p = 0.05$ in the plate, $\eta_b = 0.05$ in the beam).

These wavenumbers are related to the plate impedance and, for example, at the peaks of k_x the plate exhibits an anti-resonance (see also Figure 9 below). In the same way the nearfield wave number k_{nf} depends on the corresponding impedance of the plate which has peaks at different frequencies. At the peaks of the imaginary part of k_x the plate has a considerable damping effect on the beam.

The ratio of the imaginary part to the real part of the wavenumbers is shown in Figure 8, from which an equivalent loss factor for the coupled structure can be approximately inferred ($\eta \approx -4\,\mathrm{Im}(k)/\mathrm{Re}(k)$). The exact equivalent loss factor for the coupled beam is calculated from $\tilde{k}^4$ and given by

$$\eta = -\frac{\mathrm{Im}(\tilde{k}^4)}{\mathrm{Re}(\tilde{k}^4)}. \tag{4.16}$$

For the present case, however, because $\mathrm{Re}(\tilde{k}^4)$ and the corresponding loss factor are negative at some frequencies, the approximate equivalent loss factor is shown for convenience. Note that at the anti-resonances of the plate, this ratio can be close to 1 so that the small damping approximation no longer holds.

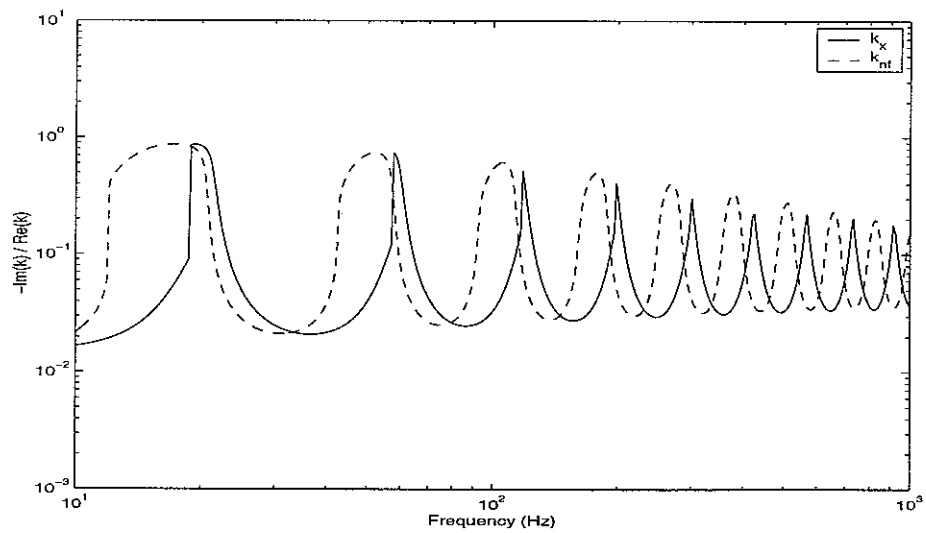

Figure 8. Ratio of the imaginary part to the real part of the travelling and the nearfield wavenumber in the coupled beam.

4.4.2 Impedance and mobilities

In Figure 9, the approximate line impedances (see equation (3.10)) of the finite width plate with damping are shown when $\tilde{k}_x$ and $\tilde{k}_{nf}$ are considered respectively.

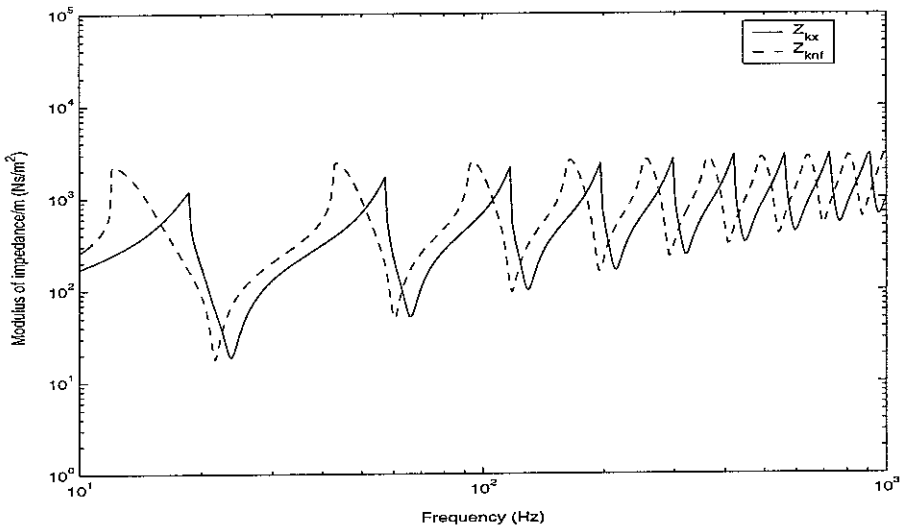

Figure 9. Approximate line impedance of the finite width plate as in Figure 3 ($\eta_p = 0.05$ in the plate) for the travelling $\tilde{k}_x$ and nearfield $\tilde{k}_{nf}$ wavenumbers in the beam.

As mentioned before, although the impedance equation (3.10) is unaltered, the figure shows how the values of the impedances are changed when $\tilde{k}_x$ or $\tilde{k}_{nf}$ is considered. The peaks in the impedance correspond to the plate anti-resonances, and comparing Figures 8 and 9, it is clear that the equivalent loss factor is maximum around these frequencies.

The point mobility of the built-up structure is shown in Figure 10 along with the corresponding FE result. Also shown is the characteristic mobility of a coupled structure consisting of a semi-infinite beam and a plate of semi-infinite length and width located in $x \geq 0$, $y \geq 0$ (dotted line). Comparing the result from the wave analysis with that from FEM, they agree quite well at low frequencies. Above 100 Hz, the resonance frequencies show differences which can be attributed to the assumption in the analytical approach that the neutral axis of the beam lies in the centre of the plate (see [1]). Nevertheless the trend is similar. The characteristic mobility passes through the centre of these results, as expected.

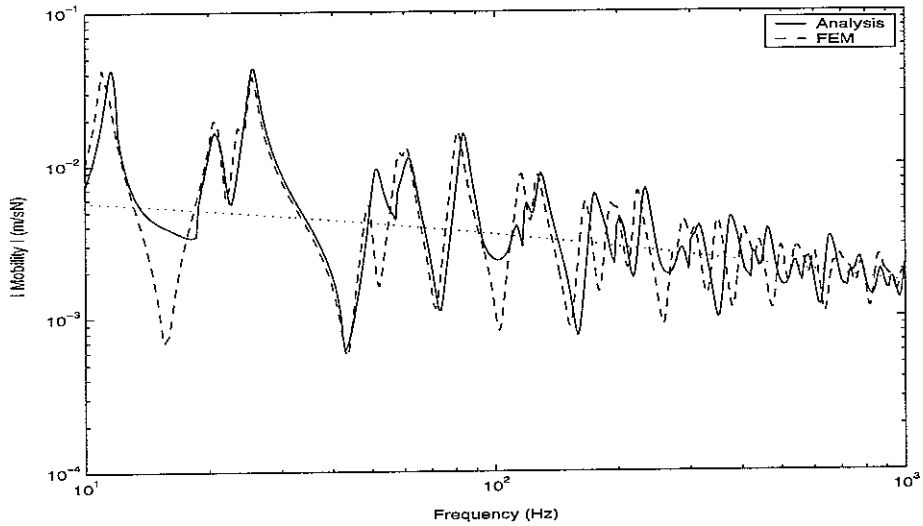

Figure 10. Point mobility of the built-up structure as in Figure 3 ($\eta_p = 0.05$ in the plate, $\eta_b = 0.05$ in the beam, point force applied at $x = 0$). Dotted line indicates characteristic mobility of a structure consisting of a semi-infinite beam and plate of a semi-infinite length and width.

Some small troughs in the analytical point mobility, for example at 18.6, 57.1, 117, 196 and 298 Hz coincide exactly with the anti-resonances of the finite width plate calculated on the basis of the travelling wavenumber $\tilde{k}_x$ (Figure 9). Note that the anti-resonances of the plate calculated using the nearfield wavenumber $\tilde{k}_{nf}$ do not appear as troughs.

By using $\tilde{k}_x$ instead of $\tilde{k}_{nf}$ in the nearfield waves in equation (4.2), the influence on the point mobility of approximating the nearfield wavenumber $\tilde{k}_{nf}$ is shown in Figure 11. Although there are some differences in the level of the peaks and troughs, this approximation seems to have only a small influence on the response of the structure. It can be assumed that $\tilde{k}_{nf}$ does not significantly affect the behaviour of the whole structure because the nearfield wave is limited to the excited region or the ends of the beam.

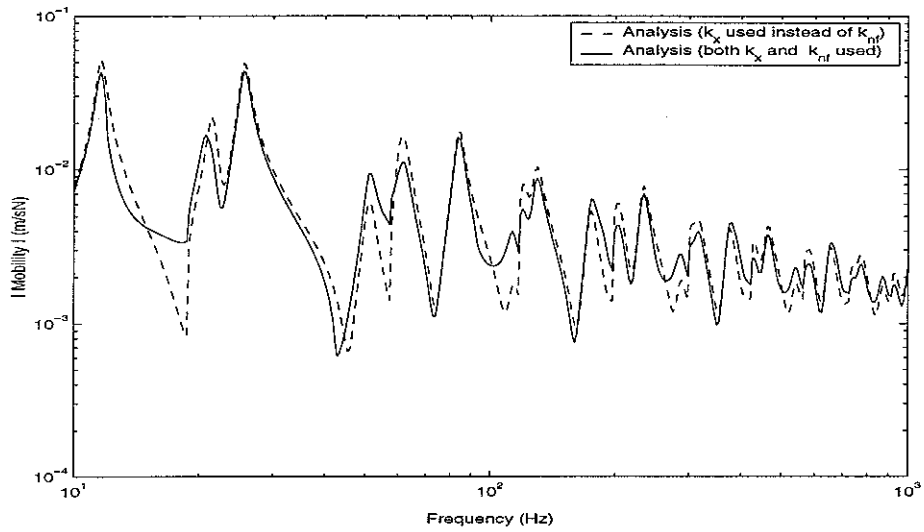

Figure 11. Point mobility of the built-up structure as in Figure 3 ($\eta_p = 0.05$ in the plate, $\eta_b = 0.05$ in the beam, point force applied at $x = 0$). Dashed line means the result when $\tilde{k}_x$ is used instead of $\tilde{k}_{nf}$ in equation (4.2) and solid line means the result when both $\tilde{k}_x$ and $\tilde{k}_{nf}$ are considered in the equation.

The point mobility of Figure 11 when $\tilde{k}_x$ is used instead of $\tilde{k}_{nf}$ in equation (4.2) is shown again in Figure 12 together with that of FEM. In some regions, such as the first trough near 18.6 Hz in the analysis, the result based on using $\tilde{k}_x$ throughout in equation (4.2) appears to give better agreement with that of FEM than the result in Figure 10 including $\tilde{k}_{nf}$. Nevertheless, comparing the results near the resonance frequencies, it can be seen that generally the result of the case when $\tilde{k}_{nf}$ is considered (Figure 10) agrees better with the FEM result than that of the case when $\tilde{k}_x$ is used throughout.

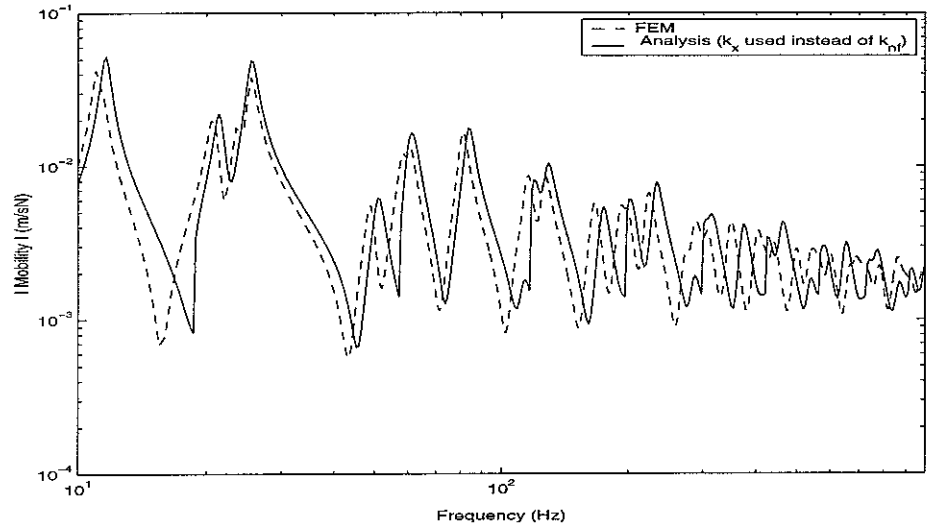

Figure 12. Point mobility of the built-up structure as in Figure 3 ($\eta_p = 0.05$ in the plate, $\eta_b = 0.05$ in the beam, point force applied at $x = 0$). The solid line indicates the result when $\tilde{k}_x$ is used instead of $\tilde{k}_{nf}$ in equation (4.2).

In Figures 13 and 14, examples of the plate response are shown. These are obtained from the sum of the results provided by the forward and backward travelling and nearfield waves as mentioned in section 4.2. Generally the level of the response agrees quite well with the FE model and the positions of the troughs in the response agree well even in the high frequency region for both figures. Nevertheless, as will be seen later by comparing the power balance for the plate, the present analysis seems to have some limitations.

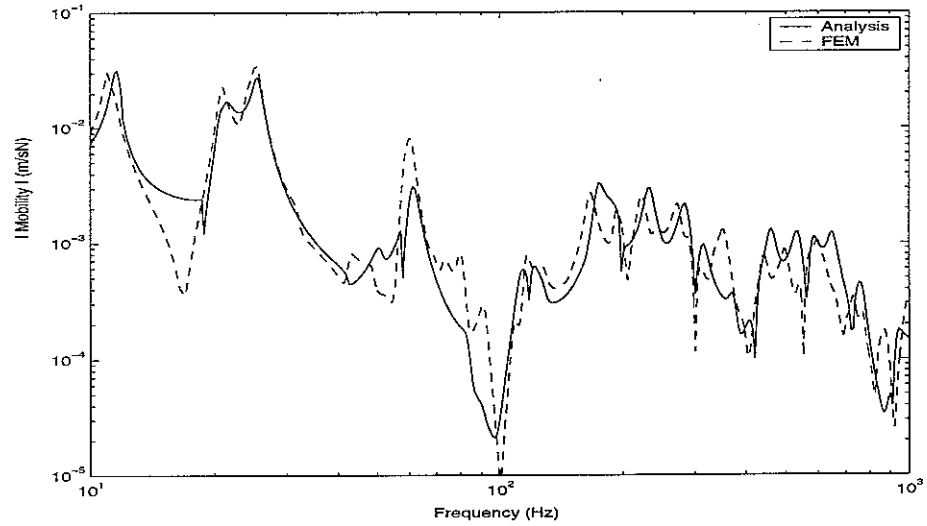

Figure 13. Transfer mobility for the plate (at x = 1.51 m and y = 0.5 m) in the built-up structure as in Figure 3 ($\eta_p = 0.05$ in the plate, $\eta_b = 0.05$ in the beam, point force applied at $x = 0$).

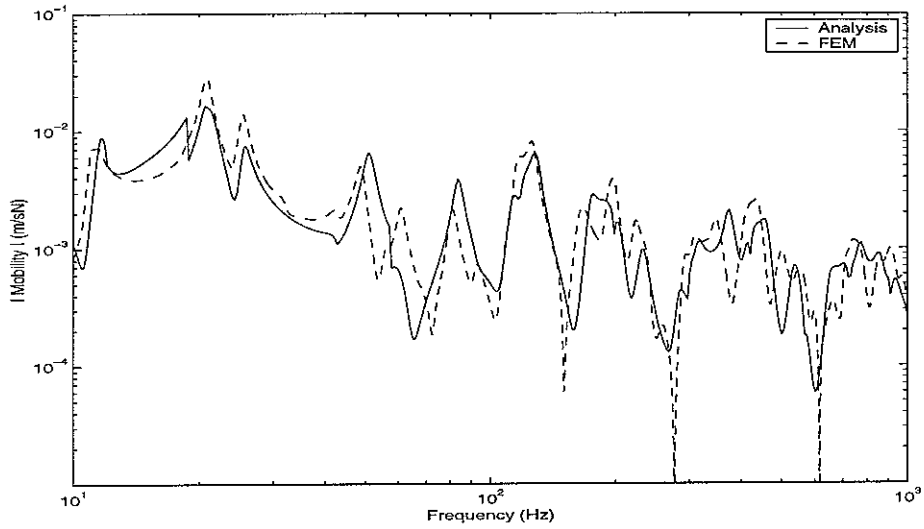

Figure 14. Transfer mobility for the plate (at x = 0.89 m and y = 0.45 m) in the built-up structure as in Figure 3 ($\eta_p = 0.05$ in the plate, $\eta_b = 0.05$ in the beam, point force applied at $x = 0$).

4.4.3 Power balance

In Figure 15, the total input power and the net power transferred to the plate are compared for the model in which the travelling wavenumber k_x and the nearfield wavenumber k_{nf} are considered separately. It is clear that the power is maximum at the resonances of the built-up structure (see Figure 10). Comparing the two powers, at peaks just above the anti-resonances of the plate, the plate receives most energy such as at the peaks at 20.9, 61.2, 120, and 201 Hz. Here the total input power and the net power transferred to the plate have almost the same values. The magnitude of the beam motion becomes larger than that of the plate at other peaks such as at 11.6, 25.4, 51.4, 83.6, and 117 Hz, and then the difference between the two powers is larger. The ratio of the power transferred to the plate to the total input power is shown in Figure 16. This has maxima close to 1 at the peaks of the plate impedance (see Figure 9) i.e. the anti-resonances of the plate.

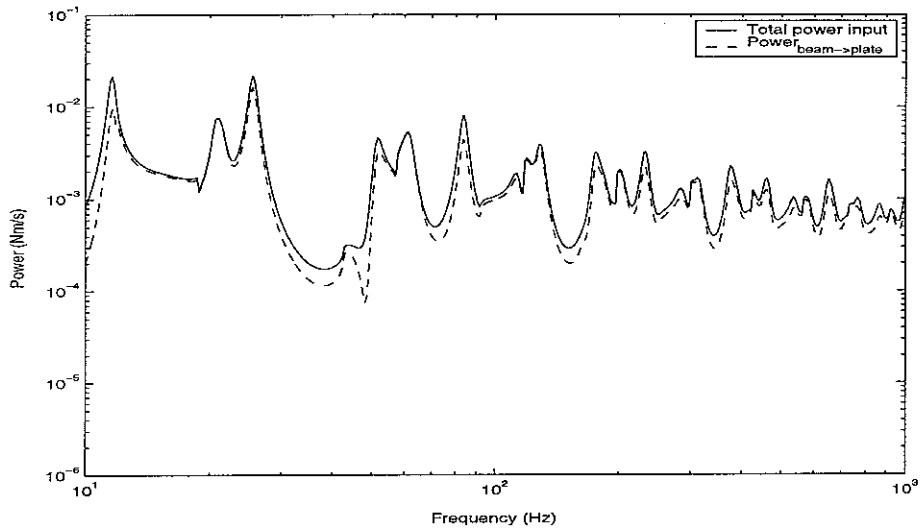

Figure 15. Comparison of total input power inserted to the built-up structure shown in Figure 3 ($\eta_p = 0.05$ in the plate, $\eta_b = 0.05$ in the beam, point force applied at $x = 0$) and net power transferred to the plate.

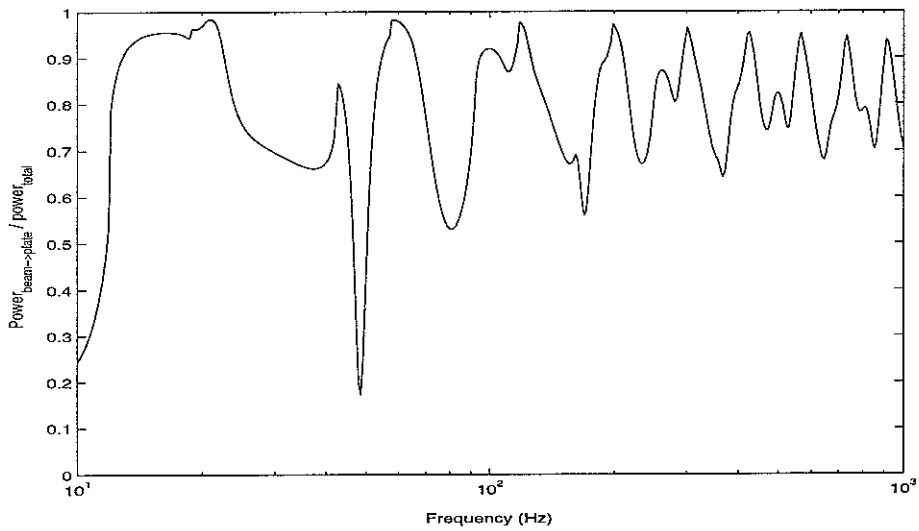

Figure 16. Ratio of the power transferred to plate to the total input power shown in Figure 15.

When the frequency corresponds to an anti-resonance of the plate, most of the power input is transferred to the plate. This is related to the high values of equivalent loss factor mentioned above. Therefore, if the equivalent loss factor has a large value (and the plate is in

anti-resonance) most of the energy is transferred from the beam to the plate and dissipated in the plate, whereas the waves in the beam decay rapidly in amplitude.

Figure 17 shows the power balance for the beam. Two identical curves are shown, indicating that the sum of the power transferred to the plate and the power dissipated by the beam is equal to the total power input to the combined structure.

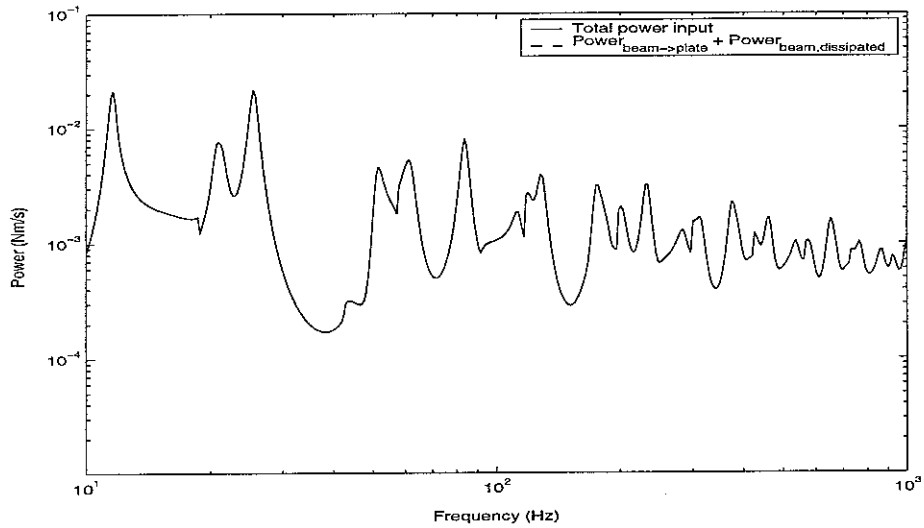

Figure 17. Comparison of power balance for beam of the built-up structure shown in Figure 3 ($\eta_p = 0.05$ in the plate, $\eta_b = 0.05$ in the beam, point force applied at $x = 0$ of beam).

Figure 18 shows the power balance for the plate. Although the power transferred to the plate is expected to be the same as the power dissipated by the plate, it can be seen that they do not agree exactly. The dissipated power is obtained from the sum of the plate responses for each of the different waves in the coupled beam and generally shows a lower level than the net power transferred to the plate.

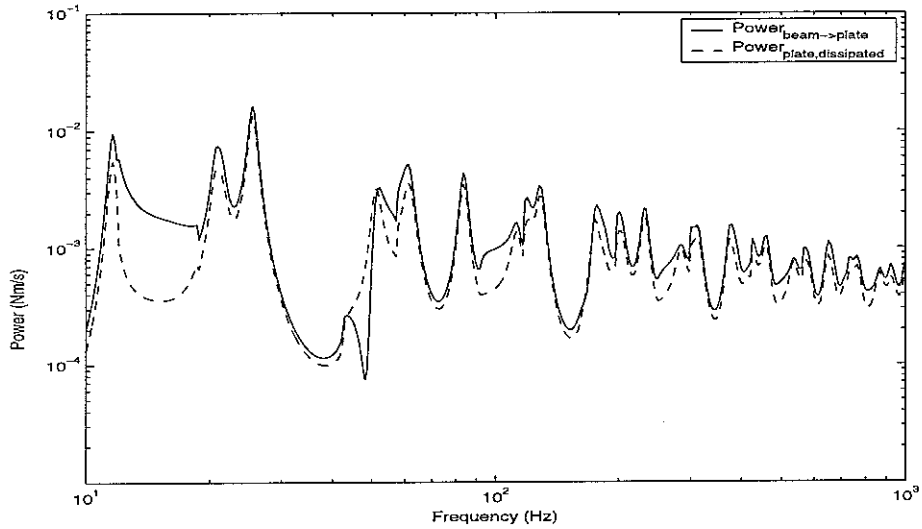

Figure 18. Comparison of power balance for the plate in the built-up structure shown in Figure 3 ($\eta_p = 0.05$ in the plate, $\eta_b = 0.05$ in the beam, point force applied at $x = 0$ of beam).

FEM can be a useful method for verification of the results shown in Figure 18. The maximum strain energy of the plate of the FEM model is obtained by the sum of the strain energies of all of the individual plate elements and the corresponding dissipated power in the plate is calculated again by using equation (4.15). The analytical results shown in Figure 18 are compared with the dissipated power of the FE model in Figures 19 and 20 respectively. Considering the troughs of the curves, especially in low frequency region, it seems that the dissipated power in the analytical model is closer to the FEM results than the transferred power. However, comparing the resonance peaks in the low frequency region and the average levels at high frequencies, it seems that the analytical model transferred power is much closer to the FE calculated dissipated power.

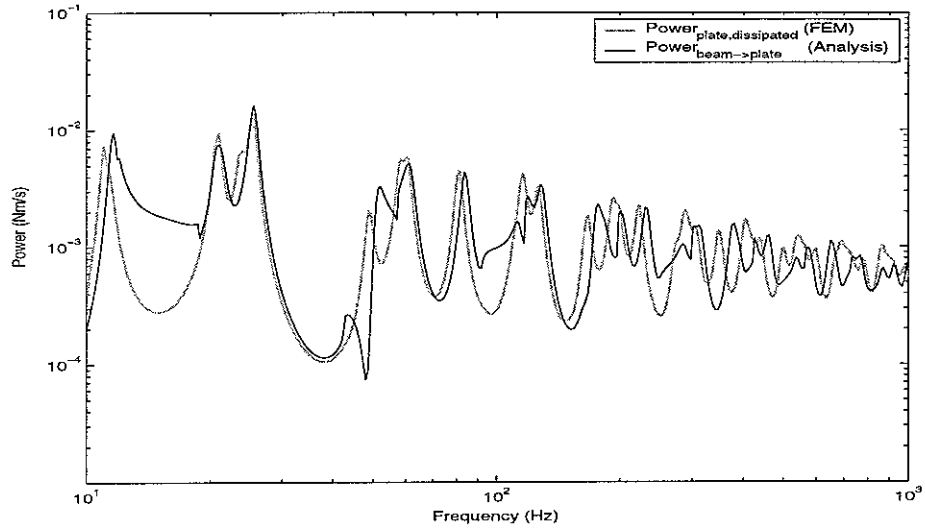

Figure 19. Comparison of power balance for the plate in the built-up structure shown in Figure 3 ($\eta_p = 0.05$ in the plate, $\eta_b = 0.05$ in the beam, point force applied at $x = 0$ of beam).

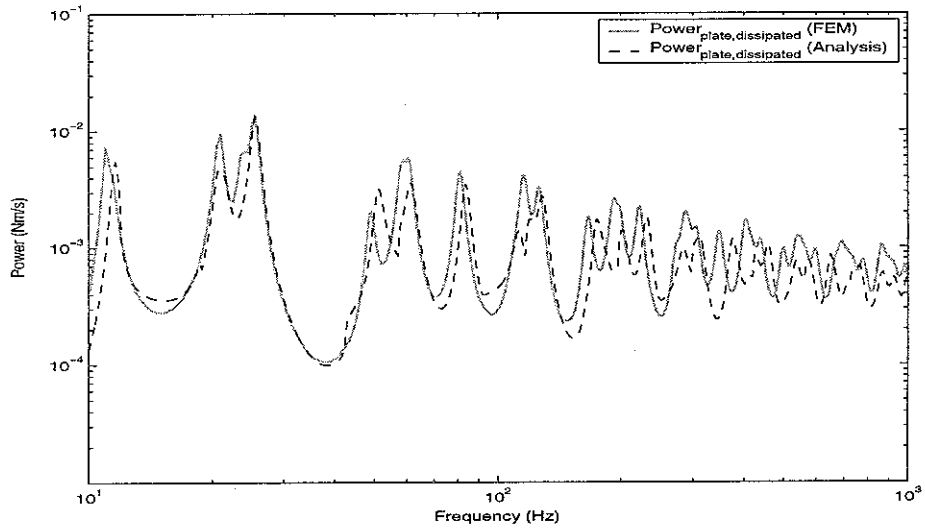

Figure 20. Comparison of the power dissipated in the plate in the built-up structure shown in Figure 3 ($\eta_p = 0.05$ in the plate, $\eta_b = 0.05$ in the beam, point force applied at $x = 0$ of beam).

The relationship becomes clearer if the ratios between the transferred power, or the dissipated power and the total input power are compared. These comparisons are shown in Figures 21 and 22. As seen in the figures, it seems clear that the agreement between the analytical transferred power (Figure 21) and the FE result is much better than is the case for the dissipated power (Figure 22). Therefore, it can be said that the analytical transferred power is closer to the exact value.

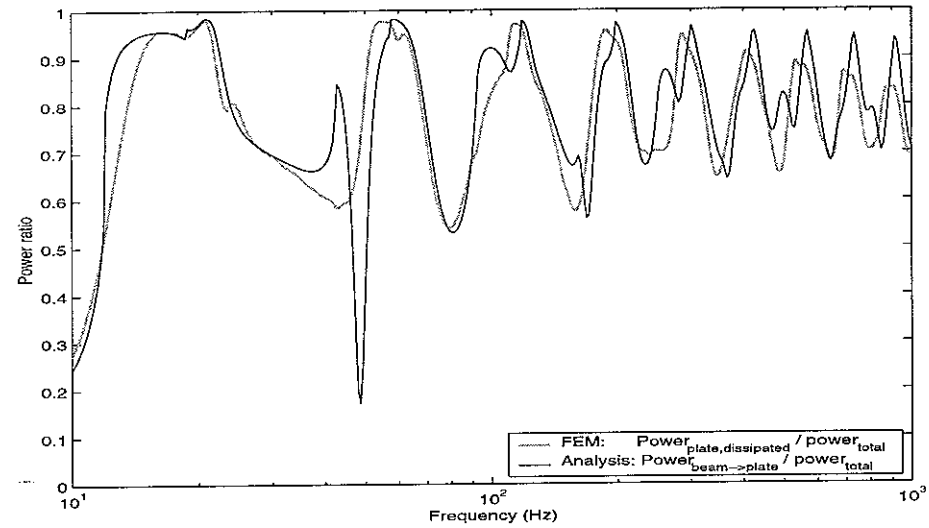

Figure 21. Comparison of power ratios ($\eta_p = 0.05$ in the plate, $\eta_b = 0.05$ in the beam, point force applied at $x = 0$ of beam).

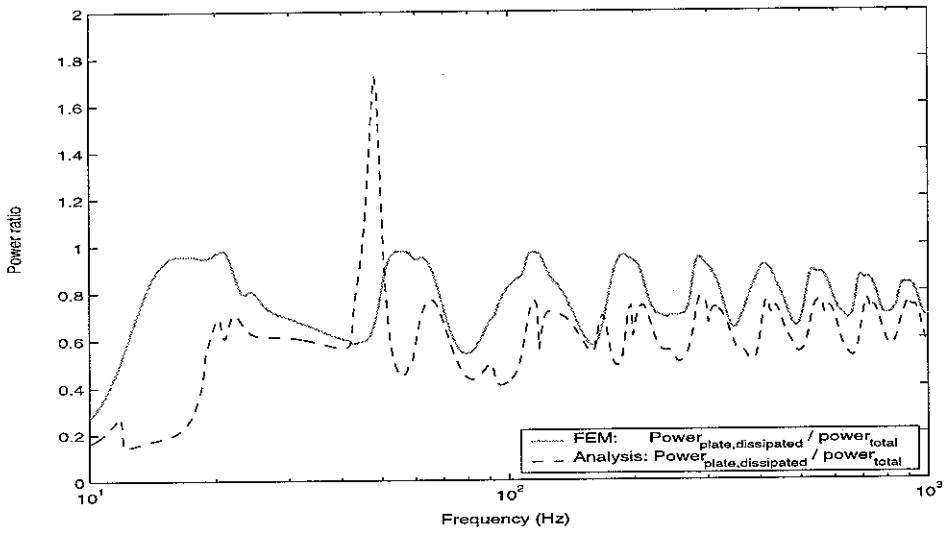

Figure 22. Comparison of power ratios ($\eta_p = 0.05$ in the plate, $\eta_b = 0.05$ in the beam, point force applied at $x = 0$ of beam).

As explained before, the four waves in the beam have been considered separately and the loading effect of the plate on the beam has been evaluated for each beam wave separately. Therefore, it seems that the behaviour of the plate cannot be separately considered in terms of the different waves of the beam, and a simple sum of the separate responses seems to be in error.

It can be shown that, although the power transferred to the plate $P_{beam\rightarrow plate}$ is different from that dissipated by the plate $P_{plate,dis}$ as in Figure 18, the transferred powers $P'_{kx,beam\rightarrow plate}$ and $P'_{knf,beam\rightarrow plate}$ calculated separately for the coupled beam wavenumbers agree with the corresponding values for the dissipated power $P'_{kx,plate,dis}$ and $P'_{knf,plate,dis}$ in the plate, calculated based on the corresponding coupled beam wavenumber. One example is shown in Figure 23, where the transferred power $P'_{kx,beam\rightarrow plate}$ and the dissipated power $P'_{kx,plate,dis}$ in the plate are compared. All of them are obtained when only the travelling wavenumber in the coupled beam and corresponding plate wavenumber are considered. They show very good agreement. Small differences in the figure seem to be due to the approximate impedance. Note that, therefore, the strain energy is obtained approximately by using the sum of the strain energy of strips, which means equation (4.14) is used instead of equation (4.12).

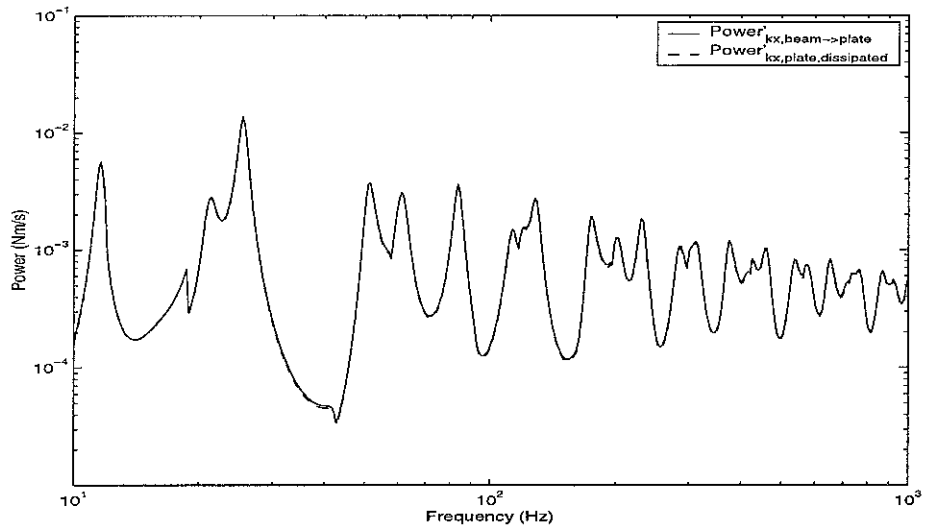

Figure 23. Comparison of power balance for the plate in the built-up structure shown in Figure 3 ($\eta_p = 0.05$ in the plate, $\eta_b = 0.05$ in the beam, point force applied at $x = 0$ of beam).

Both results are calculated when only $\tilde{k}_x$ is used in the power calculation. Hence it is found that

$$P_{beam\rightarrow plate} \neq P_{plate,dis} \tag{4.17}$$

but

$$P'_{kx,beam\to plate} = \frac{1}{2}\int_0^{L_x} \mathrm{Re}\left\{\left(\tilde{V}_{beam,kx}\tilde{Z}'_{p,kx}\right)^* \tilde{V}_{beam,kx}\right\}dx = P'_{kx,plate,dis}$$
$$P'_{knf,beam\to plate} = \frac{1}{2}\int_0^{L_x} \mathrm{Re}\left\{\left(\tilde{V}_{beam,knf}\tilde{Z}'_{p,knf}\right)^* \tilde{V}_{beam,knf}\right\}dx = P'_{knf,plate,dis} \quad (4.18)$$

Thus if only one wave type is present in the beam, the power balance holds. It seems that the calculation of the plate response based on the separation of the coupled wavenumber has some limitation and further investigation is required. On the other hand, the good agreement found in Figure 17 suggests that $P_{beam\to plate}$ could be used as an estimate of the power dissipated in the plate.

4.5 Numerical analysis - plate in sliding condition

In the previous section, numerical calculations were given for the case when the opposite edge of the plate parallel to the beam is pinned, giving a reflection coefficient $\tilde{r} = -1$. In this section, only the boundary condition shown in Figure 3 is changed from the pinned to the sliding condition which means $\tilde{r} = +1$. Basically the characteristics of physical phenomena, for example the relationship between the wavenumbers and the plate impedance and the damping effect of the plate at its anti-resonances are the same as those in the previous section. Therefore, only the values of, for example, the resonance frequencies and the anti-resonance frequencies in the impedance will be changed due to the change of the reflection coefficient. Nevertheless, it is important to include the responses of the structure for a sliding plate condition. This is because this structural analysis can be used in the analysis of more complicated structures, for example the structure consisting of two beams which will be discussed later in this report with its response related to those of the present system. The numerical results are presented following the same procedure as that in the previous section.

4.5.1 Wavenumbers

Figure 24 and Figure 25 show the wavenumber in the coupled beam and the corresponding

wavenumber in the plate. They show that the assumption of the approximate impedance is still valid for the sliding boundary condition, as $\left|\tilde{k}_x\right| \ll k_p$ and $\left|\tilde{k}_{nf}\right| \ll k_p$.

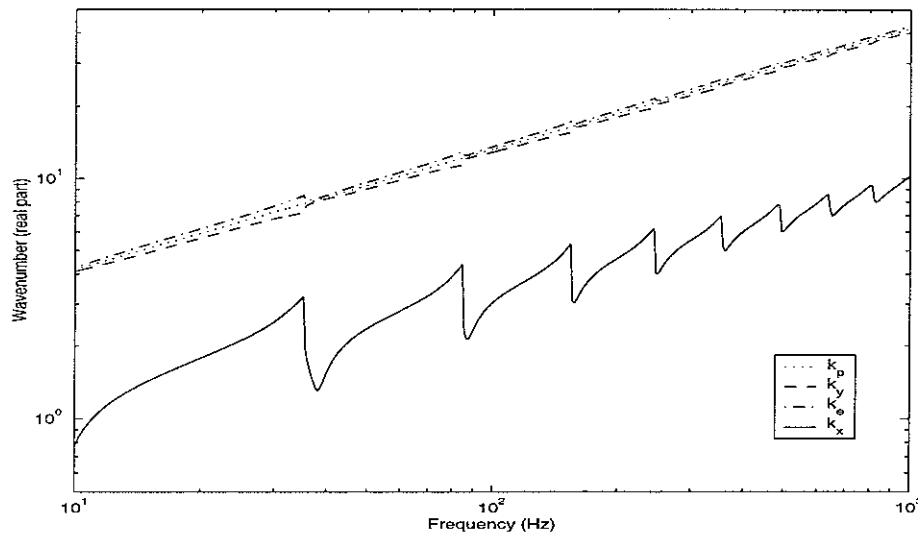

Figure 24. Comparison of the travelling wavenumber of the beam and the corresponding wavenumbers of the plate of the built-up structure as in Figure 3 but with a sliding condition on the edge opposite to the beam (real part only, $\eta_p = 0.05$ in the plate, $\eta_b = 0.05$ in the beam).

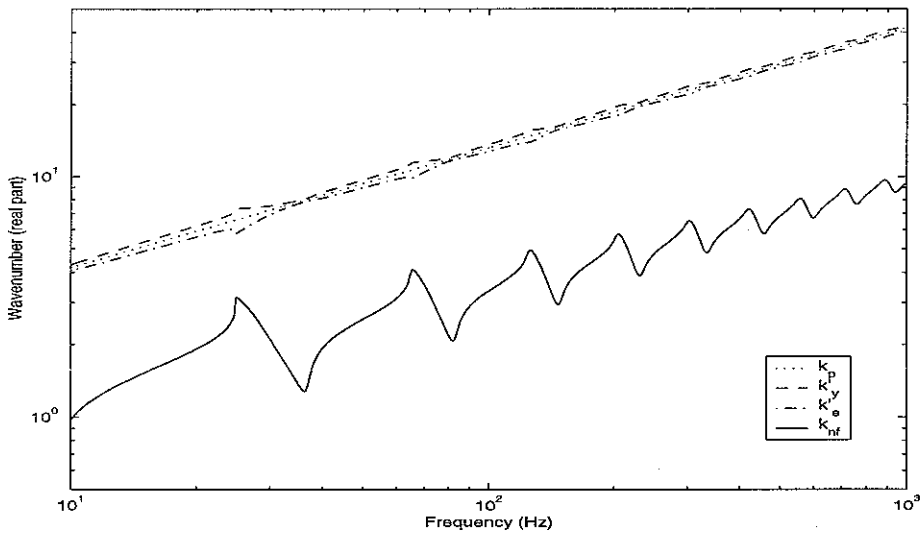

Figure 25. Comparison of the nearfield wavenumber of the beam and the corresponding wavenumbers of the plate of the built-up structure as in Figure 3 but with a sliding condition on the edge opposite to the beam (real part only, $\eta_p = 0.05$ in the plate, $\eta_b = 0.05$ in the beam).

Figure 26 shows the complex travelling wavenumber and nearfield wavenumber of the coupled beam. Although the frequencies of the peaks themselves are different from the case of the pinned condition, the relationship between the wavenumber and the impedance is the same as in the pinned condition (see also Figure 28). Also, the ratio of the imaginary part to the real part of the wavenumber is shown in Figure 27 which corresponds to an equivalent loss factor as before.

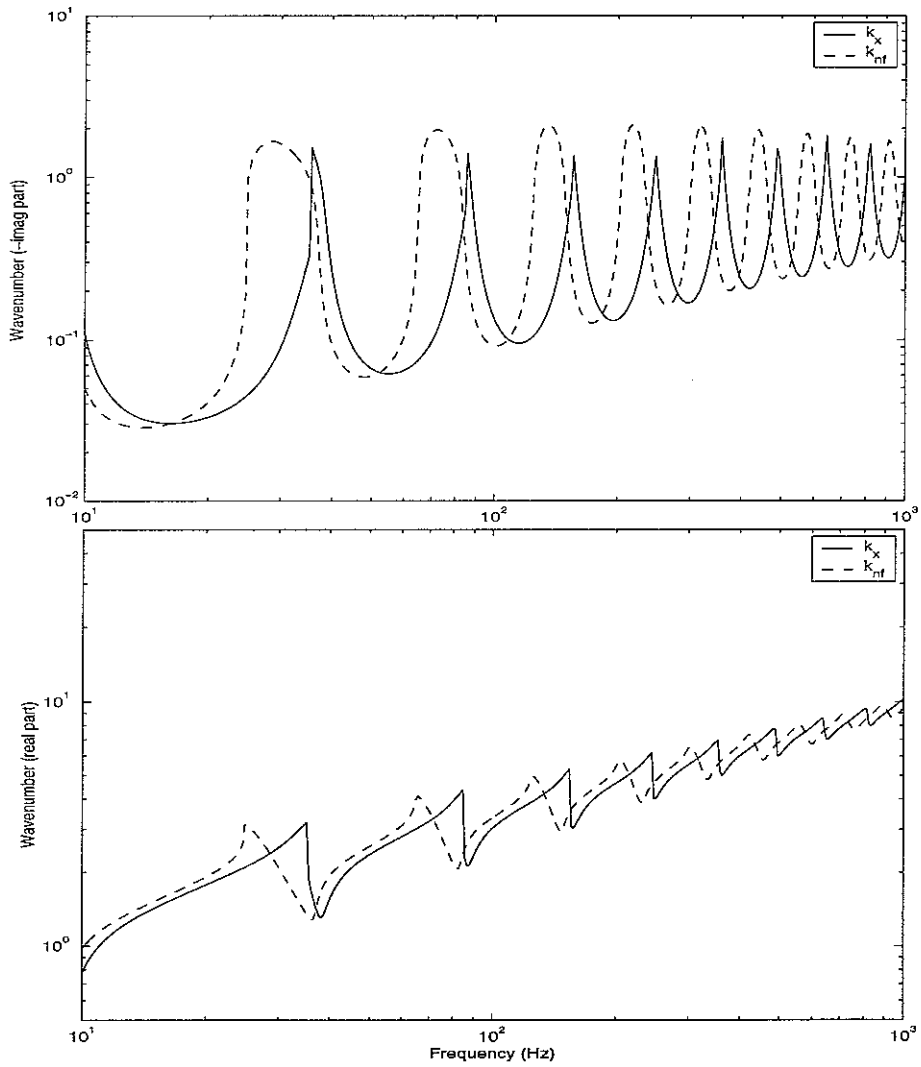

Figure 26. Comparison of the beam travelling and the nearfield wavenumber of the built-up structure as in Figure 3 but with a sliding condition on the edge opposite to the beam.

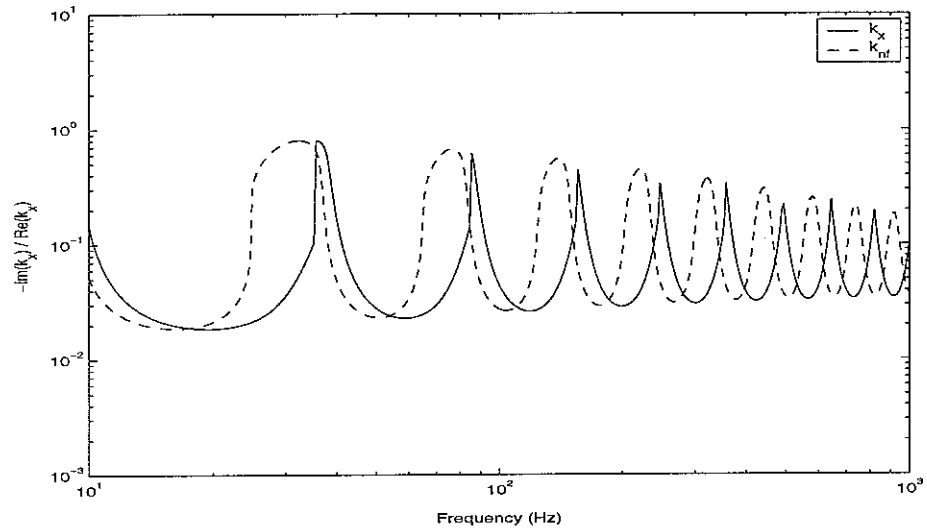

Figure 27. Ratio of the imaginary part to the real part of the travelling and the nearfield wavenumber in the coupled beam.

4.5.2 Impedance and mobilities

In Figure 28 the approximate impedance of the finite plate with damping is shown when the corresponding travelling and nearfield wavenumbers in the coupled beam are considered separately. Anti-resonance frequencies of the impedance due to the travelling wavenumber k_x, for example at 35.1, 84.5, 154 and 245 Hz, coincide with the frequencies of the peaks in Figure 26.

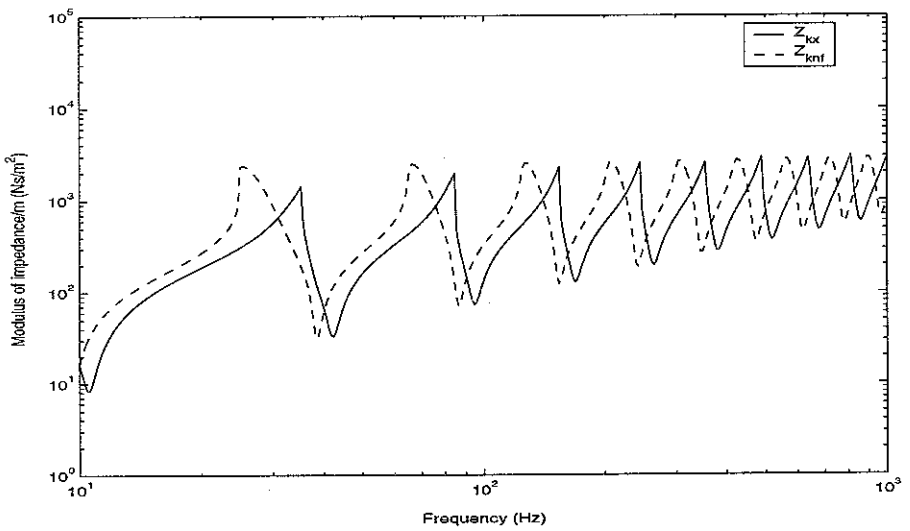

Figure 28. Approximate impedance of the finite plate as in Figure 3 but with a sliding condition on the edge opposite to the beam ($\eta_p = 0.05$ in the plate)

The point mobility of the built-up structure for this configuration is shown in Figure 29. The peaks in the plate impedance result in small troughs in the overall point mobility. The result from the analysis and that from FEM agree well at low frequencies and their levels at high frequencies are similar on average, the difference in natural frequencies again being due to the assumption about the position of the beam neutral axis.

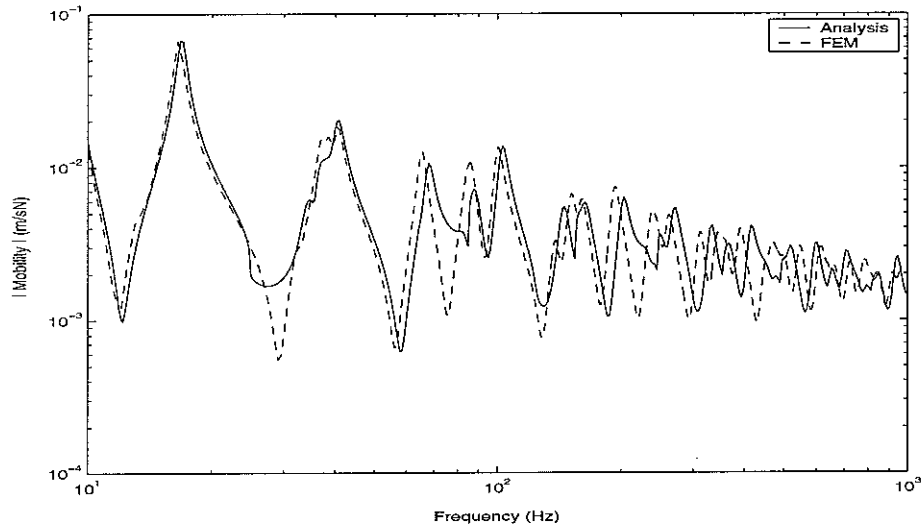

Figure 29. Point mobility of the built-up structure with the sliding condition ($\eta_p = 0.05$ in the plate, $\eta_b = 0.05$ in the beam, point force applied at $x = 0$). FEM results are shown for comparison.

Another analytical result is shown in Figure 30, which is the point mobility when the travelling wavenumber $\tilde{k}_x$ is used instead of the nearfield wavenumber $\tilde{k}_{nf}$ in the beam response (equation (4.2)). As in the pinned structure case, it seems that both analytical results are similar, but comparing the resonance frequencies, the result when $\tilde{k}_{nf}$ is considered seems to be closer to that of the FEM model, whereas the troughs are represented more reliably using only $\tilde{k}_x$.

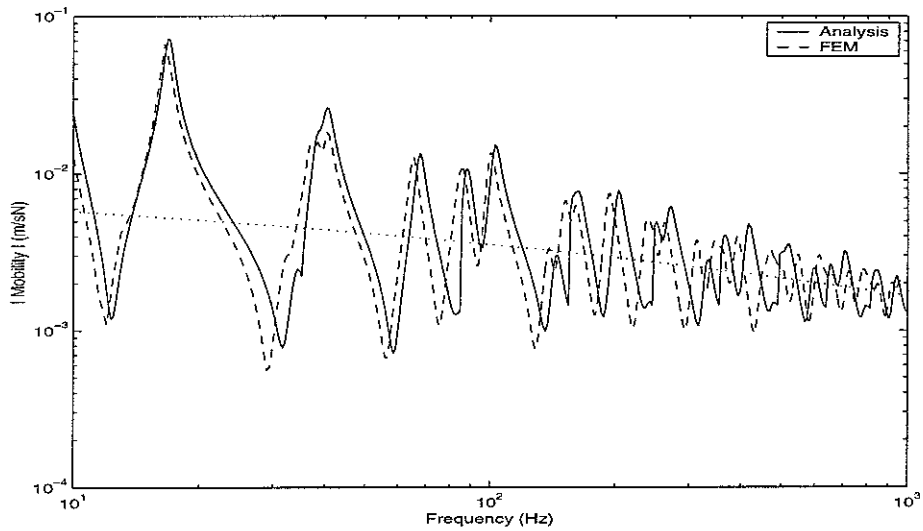

Figure 30. Point mobility of the built-up structure with the sliding condition ($\eta_p = 0.05$ in the plate, $\eta_b = 0.05$ in the beam, point force applied at $x = 0$). Solid line represents the result when $\tilde{k}_x$ is used instead of $\tilde{k}_{nf}$ in equation (4.2).

4.5.3 Power relationship

The relationship between the power input and the power transferred to the plate and their ratio are shown in Figure 31 and Figure 32 respectively.

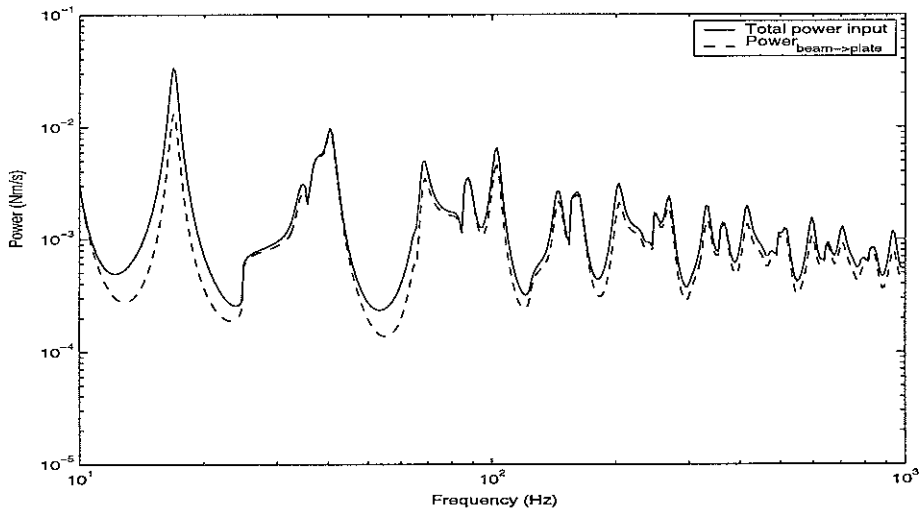

Figure 31. Comparison of input power and transferred power in the built-up structure for the sliding edge condition ($\eta_p = 0.05$ in the plate, $\eta_b = 0.05$ in the beam, point force applied at $x = 0$).

As explained for the pinned structure case, at the anti-resonance frequencies of the plate, such as 35.1, 84.5, 154 and 245 Hz, most power is transferred to the plate. These frequencies again coincide with those of the peaks of the equivalent loss factor based on the travelling wavenumber k_x shown in Figure 27.

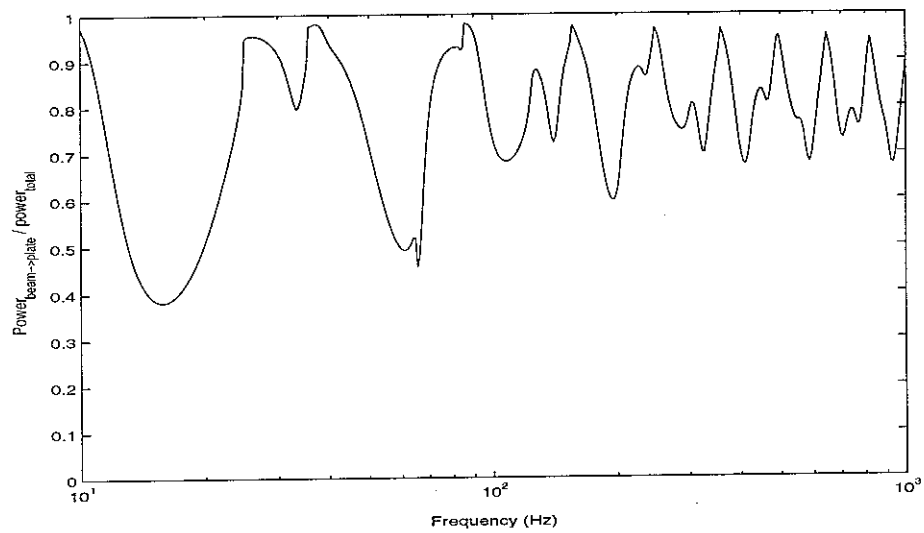

Figure 32. Ratio of the power transferred to plate to the total input power shown in Figure 31.

5. Two parallel beams coupled to finite plate in a symmetric configuration

5.1 Synthesis from non-symmetric structure

A symmetric structure consisting of two identical beams and single rectangular plate is examined here. In principle, the analysis performed and the results found should give some indication of the behaviour of a fully framed plate structure. Although the latter is a more complicated configuration, for example at the joint where two beams and a plate meet, the interaction between the plate and beams may be expressible using similar assumptions for the framed structure.

Consider a framed structure consisting of four beams that are identical apart from their lengths, attached along all four edges of a rectangular plate. If it can be assumed that all of the beams have infinite torsional stiffness, then the ends of them experience sliding boundary

conditions. If two opposite beams are removed and a point force is applied at one end of the beam, then the structure will be as shown in Figure 33. All of the dimensions follow Table 1 and the width of the plate ($2L_y$) is 1.5 m.

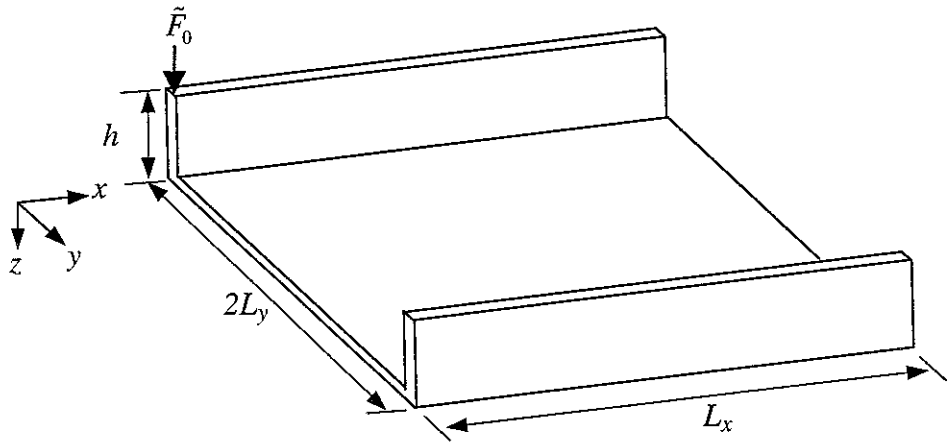

Figure 33. A built-up structure consisting of two finite beams attached to a rectangular plate.

As the torsional stiffness of the beams is infinite, the edges of the plate attached to the beams also have a sliding boundary condition. Now, by symmetry, the wave motion in the plate generated by the forced beam can be described by a combination of the waves reflected by a pinned condition along the centre line of the plate, parallel to the beam ($y = L_y$), and the waves reflected by a sliding condition along the same line. Therefore, the analysis performed for the structure consisting of one beam and one plate in the previous sections can be used in this analysis. No constraints are required at the other two edges of the plate without beams, because in the present case the plate is assumed to behave like independent strips.

Figure 34 shows how the response of the symmetric structure, excited by a force on one side, can be synthesized from a combination of the motion of the structure which is antisymmetric and that which is symmetric about the middle line ($y = L_y$) of the plate.

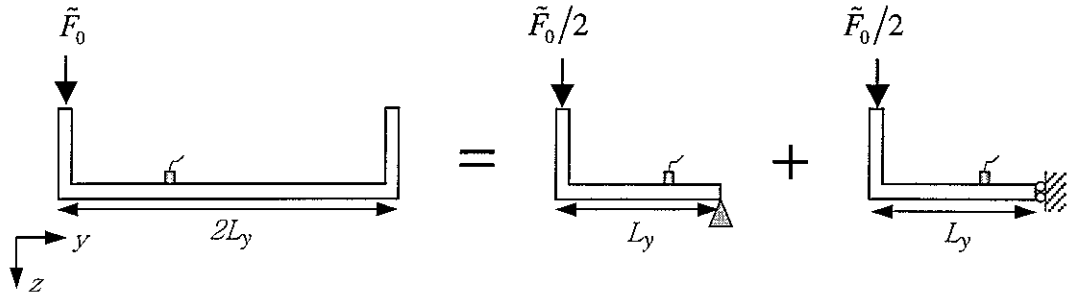

Figure 34. Response of a symmetric structure given in Figure 33 calculated from consideration of the antisymmetric and symmetric motion.

If the point force is applied at the end of the beam (beam 1) of the symmetric structure, the response of the left side ($0 \le y \le L_y$) of the structure can be assumed to be the sum of the antisymmetric response of the structure with a pinned condition and the symmetric response of the same structure with a sliding condition at $y = L_y$. Meanwhile, the response of the right side ($L_y \le y \le 2L_y$) can be obtained from the difference between the results.

$$\tilde{Y}_{sum} = \frac{\tilde{Y}_{pin} + \tilde{Y}_{sliding}}{2} \quad (\text{for } 0 \le y \le L_y),$$
$$\tilde{Y}_{sum} = \frac{-\tilde{Y}_{pin} + \tilde{Y}_{sliding}}{2} \quad (\text{for } L_y < y \le 2L_y). \tag{5.1a,b}$$

The force acting on the plate from the beam can be calculated from the transfer mobility of the beam and the approximate plate impedance for the corresponding boundary condition. For example, the force acting on the plate from beam 1 of the synthesized structure can be expressed in the form of

$$\tilde{F}(x) = \frac{\tilde{F}_0}{2}\left(Y_{beam1,pin}(x) \times Z'_{p,pin} + Y_{beam1,sliding}(x) \times Z'_{p,sliding}\right). \tag{5.2}$$

The force acting on the right-hand beam of the structure (beam 2) can also be calculated in the same way. No net external force acts on beam 2 as the forces in the two component models cancel.

While such an approach is commonly used, for example in FEM [5], it should be realised that the coupled wavenumbers in the two component models differ, as they depend on different line impedances. The assembly from symmetric and antisymmetric models, therefore represents an approximation in the present analysis.

5.2 Power balance of the subsystems

The concept of power balance, discussed in section 4.3, can be extended to the structure consisting of two beams as in Figure 33 and is shown in Figure 35. Because the external force is applied only to beam 1, the power flows from beam 1 to beam 2 through the plate and the power flowing between the subsystems such as $P_{beam1\rightarrow plate}$ represents the net transferred power. Note that the dissipated power in the plate should be the difference between the power transferred from beam 1 to the plate and the power transferred from the plate to beam 2. The dissipated power in each subsystem is calculated in the same way as described in section 4.3.

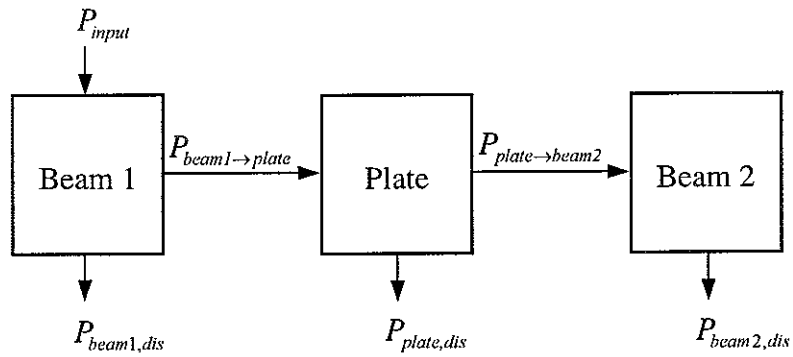

Figure 35. Power balance between subsystems of the coupled structure as in Figure 33.

5.3 Numerical analysis

The point mobility of the combined structure, calculated using equation (5.1a), is shown in Figure 36. Comparing it with corresponding results from FEM, generally close agreement is found. The mobility contains dynamic characteristics of both the pinned and sliding systems; for example the peaks at 11.6, 25.4, and 51.4 Hz correspond to the resonance frequencies of the pinned system (Figure 10) and those at 16.8, 40.4, and 68.7 Hz are the resonance frequencies of the sliding system (Figure 29). The former modes correspond to anti-symmetric behaviour of the whole structure, and the latter to symmetric behaviour. Also, it can be seen that the plate impedances corresponding to the travelling wave k_x (Figures 9 and 28) have an influence on the synthesized structure as well. At the anti-resonance frequencies 57.1, 117 and 298 Hz of the pinned plate and 154 and 245 Hz of the sliding plate, the point mobility of the combined system has small troughs. Some of the anti-resonances seem to have no influence on the response of the structure, but this is because the response is described by the sum of the two structures with different boundary conditions. For example, the anti-resonance of the sliding structure at 84.5 Hz does not result in any trough because the response is dominated by the resonance of the pinned structure at 83.6 Hz.

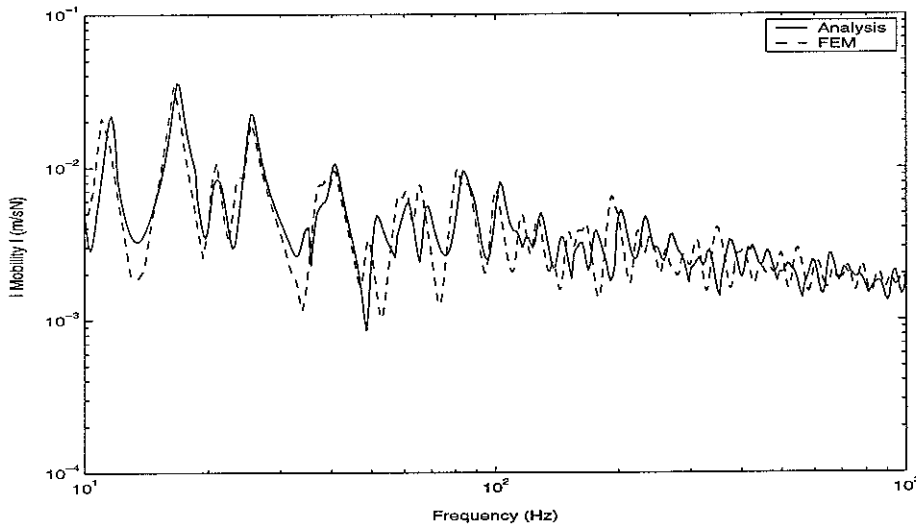

Figure 36. Point mobility of the symmetric built-up structure as in Figure 33 ($\eta_p = 0.05$ in the plate, $\eta_b = 0.05$ in the beam, point force applied at $x = 0$ of beam 1).

Figure 37 shows the total input power and the power transferred between the subsystems. Comparing the total power of the synthesized system with that of the non-symmetric systems (Figures 15 and 31), it can be seen that the power includes the characteristics of both the pinned and sliding conditions. The power transferred to the plate from beam 1 is mostly more than a factor of 10 (10 dB) greater than the power transferred to beam 2 from the plate. The difference between these two values can be considered to be the power dissipated in the plate, which will be discussed later.

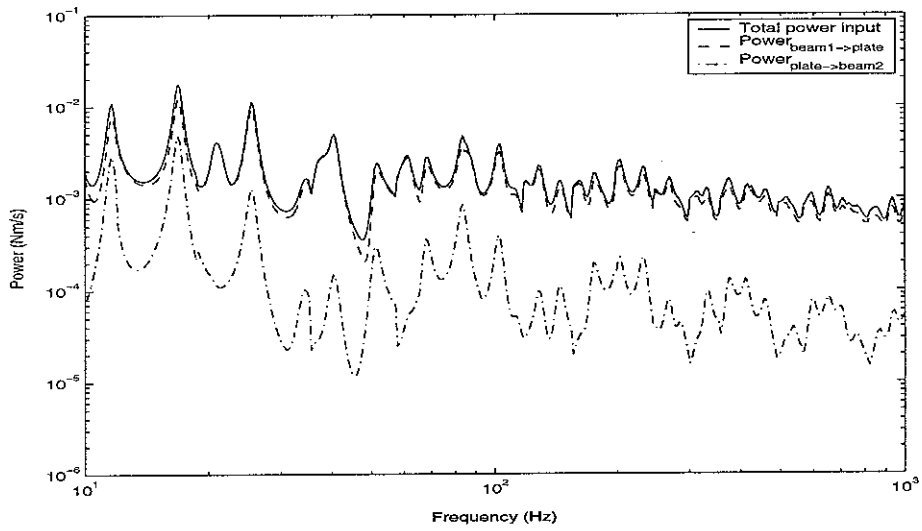

Figure 37. Comparison of total input power to the symmetric built-up structure as in Figure 33 and the net power transferred to the plate ($\eta_p = 0.05$ in the plate, $\eta_b = 0.05$ in the beam, point force applied at $x = 0$ of beam 1).

In Figure 38, the total power and the sum of the power transferred to the plate and the power dissipated in beam 1 are compared. They show that the power input is completely accounted for by the power transferred from beam 1 to the plate and the dissipated power of beam 1.

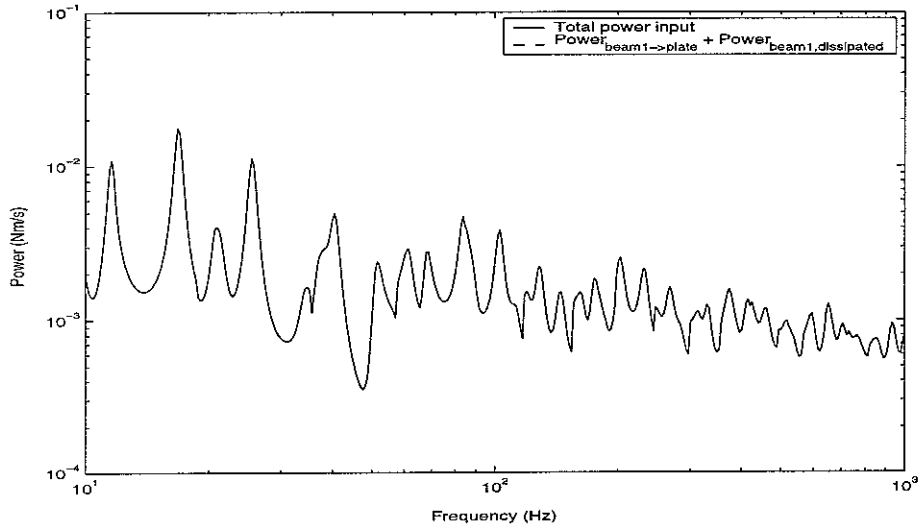

Figure 38. Comparison of power balance for beam 1 ($\eta_p = 0.05$ in the plate, $\eta_b = 0.05$ in the beam, point force applied at $x = 0$ of beam 1).

In the same way as for the power balance for beam 1, the power transferred into beam 2 should equal the power dissipated in this beam. Figure 39 shows these two quantities. Although in most regions they agree well, it can be seen that there are small differences at some low frequency minima such as at 30.9, 35.5 and 45.3 Hz.

The plate impedances are changed because of different boundary conditions along the edge of the plate and, therefore, the coupled wavenumbers in the two component models differ. Therefore, although the synthesis explained in section 5.1 is a common procedure, for example in FEM [5], it seems that there is some limit in calculating the exact response of beam 2 based on the coupled wavenumber of beam 1. That is, the coupled wavenumber of beam 2 due to the plate coupling does not seem to be exactly the same as that of beam 1, and therefore, this limits the accuracy of the response of beam 2 obtained using the symmetric and antisymmetric responses.

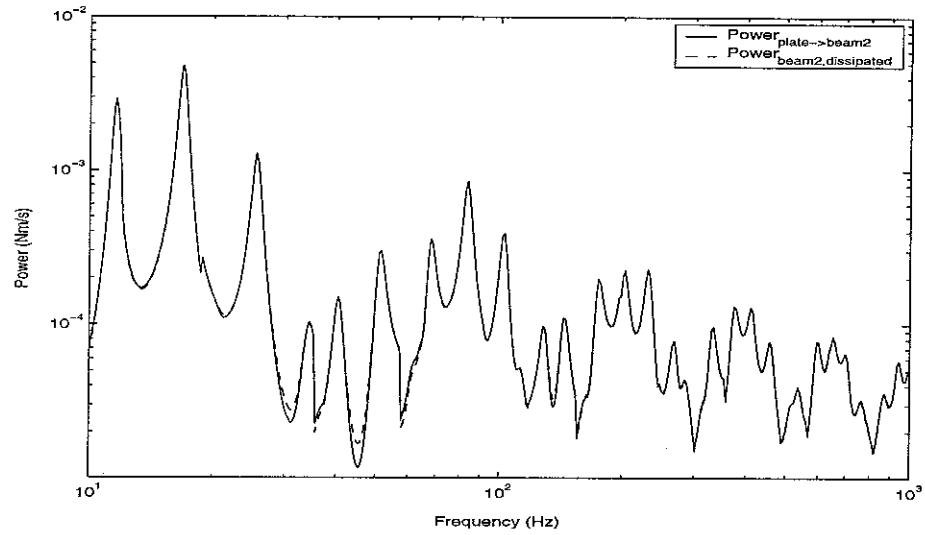

Figure 39. Comparison of power balance for beam 2 ($\eta_p = 0.05$ in the plate, $\eta_b = 0.05$ in the beam, point force applied at $x = 0$ of beam 1).

Concerning power balance for the plate, although the dissipated power in the plate is expected to be the same as the net power transferred to the plate, Figure 40 shows that the power balance does not agree.

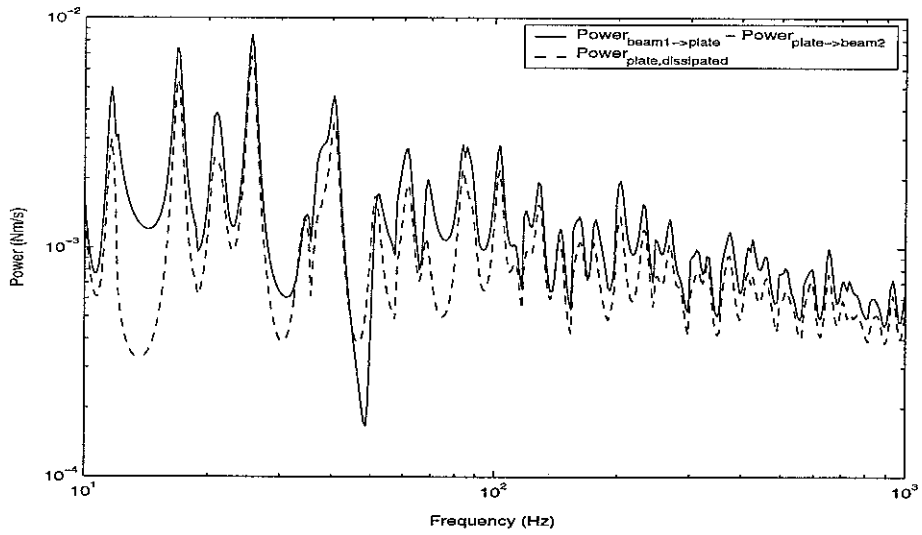

Figure 40. Comparison of power balance for the plate ($\eta_p = 0.05$ in the plate, $\eta_b = 0.05$ in the beam, point force applied at $x = 0$ of beam 1).

The reason for this discrepancy was already explained in section 4.4. The difference seems larger than before and is probably due to the combined effect of using the summation of both the symmetric and antisymmetric response of the structure as well as having a different impedance and wavenumber for the travelling and nearfield waves.

6. Conclusions

The procedure for the calculation of the coupled wavenumber mentioned in the previous report [1] has been reviewed and the non-convergence of the wavenumber in the iteration procedure at certain frequencies has been explained. As an alternative numerical approach, it has been shown that Muller's method can be applied to obtain the complex coupled wavenumber based on the dispersion equation.

The general relationship between the coupled beam wavenumber and the plate wavenumber has been derived when the nearfield wavenumber in the coupled beam is considered, and the corresponding plate impedance has been explained. This shows that the impedance equation is not changed regardless of wave types but the numerical values for the impedance are changed.

Comparing the analytical results with those from FEM, it is seen that they agree closely when the coupled waves are considered separately. Also, comparing the influence of the anti-resonance of the plate due to the different wave types, it has been shown that the dynamic characteristics of the coupled structure depend mainly upon the travelling wave. This can be confirmed when the travelling wavenumber is substituted for the nearfield wavenumber, instead of the latter being evaluated separately.

The power relationship reported previously [1] has been developed to consider the power balance for the coupled structure consisting of a single beam and a plate. The power balance for the beam is in good agreement, but for the plate there is some difference between the

results for the power transferred to the plate and its dissipated power. When only one wave type in the beam is considered separately they show good agreement. Therefore, it seems to occur because the plate responses are calculated in terms of separate beam wave types, the beam wavenumbers also being calculated independently. This problem requires further study.

Numerical results are also shown for the case when the plate edge of the non-symmetric structure, consisting of a single beam and a plate, has a sliding condition instead of the pinned condition. Using a combination of these two non-symmetric models, an analysis of a symmetric beam-plate-beam structure was synthesized when one of the beams is excited. The response of the synthesized model shows features from both the symmetric and antisymmetric response.

Good agreement is found between the point mobility of the symmetric beam-plate-beam system obtained with the present method and that from FEM. Nevertheless, it seems that there is some limit in obtaining accurate responses using this synthesis method. The power balance for the undriven beam, the wavenumbers of which are calculated on the basis of the symmetric and antisymmetric responses, shows some discrepancies while that for the plate shows quite substantial differences.

Concerning further study, it is proposed to study the system of two beams coupled to a plate using a Fourier transform technique [6]. This allows the behaviour to be constructed from forced vibration at all wavenumbers rather than concentrating on the free wavenumbers. It should also allow two dissimilar beams to be considered. The behaviour at a corner, where two beams and a plate meet, is also a necessary consideration in further activities in order to describe the response of a framed plate.

References

1. J. W. Yoo, N. S. Ferguson and D. J. Thompson 2002 *ISVR Memorandom No*:**888**. Structural analysis of a combined beam and plate structure using a wave approach.

2. G. B. Warburton 1976 *The Dynamical Behaviour of Structures*. Oxford: Pergamon Press; second edition.

3. S. P. Timoshenko and S. Woinowsky-Krieger 1959 *Theory of plates and shells*, New York: McGraw-Hill; second edition.

4. R. H. Lyon and R. G. Dejong 1995 *Theory and Application of Statistical Energy Analysis*. Boston: Butterworth-Heinemann.

5. M. Petyt 1990 *Introduction to finite element vibration analysis*. Cambridge: Cambridge University Press.

6. L. Ji, B. R. Mace and R. J. Pinnington 2002 *ISVR Memorandom No*:**877**. Power transmission to flexible receivers by force sources.

7. C. F. Gerald 1977 *Applied Numerical Analysis*, San Luis Obispo.

8. R. M. Grice and R. J. Pinnington 1999 *Journal of Sound and Vibration* **230**, 825-849. A method for the vibrational analysis of built-up structures, part 1: Introduction and analytical analysis of the plate-stiffened beam.

9. L. Cremer, M. Heckl and E. E. Ungar 1988 *Structure-borne Sound*. Berlin: Springer Verlag; 2nd edition.

10. D. J. Thompson 2002 "*ISVR Short Course Lecture notes on High Frequency Modelling of Structural Vibration*", ISVR, Southampton

Appendices

Appendix A. Nomenclature

A	wave amplitude in a beam (m)
B	wave amplitude in a plate (m)
C	wave amplitude in a plate (m)
D	beam stiffness (Nm^2); plate stiffness (Nm)
E	Young's modulus of elasticity (N/m^2); energy
f	frequency (Hz)
F	force per unit length (N/m)
h	height of a beam
i	$\sqrt{-1}$
k_b	uncoupled beam wavenumber
k_e	nearfield trace wavenumber in a plate
k_{nf}	coupled nearfield trace wavenumber of a beam
k_p	uncoupled free wavenumber in a plate
k_x	coupled travelling trace wavenumber of a beam
k_y	travelling trace wavenumber in a plate
L_x	length of a beam (m)
L_y	width of a plate (m)
m_b'	mass per unit length of a beam (kg/m)
m_p''	mass per unit area of a plate (kg/m^2)
P	power
$\tilde{r}$	reflection coefficient (-)
t	thickness (m); time
V	velocity response (m/s)
w	displacement (m)
x, y, z	co-ordinates

Y	structural mobility (m/sN)
Z'	structural impedance per unit length (Ns/m^2)
$\tilde{\beta}$	travelling wave attenuation coefficient (-)
η	structural loss factor (-)
ν	Poisson's ratio
ρ	density (kg/m^3)
ω	radian frequency (rad/s)

Appendix B. Use of Muller's method for the estimation of coupled wavenumbers

Previously [1], the coupled wavenumber k_x was calculated iteratively and erratic fluctuations in the coupled wavenumber and corresponding plate impedance at some frequencies were observed. In this appendix, the iteration procedure is explained briefly and a numerical procedure is described to eliminate these fluctuations.

Consider the same structure consisting of a finite width plate and an infinite beam shown in section 3.1 (see Figure 2). Corresponding dimensions are the same as those shown in Table 1. A pinned boundary condition along the opposite edge parallel to the beam is considered and the beam is also assumed to be infinitely stiff in torsion.

The coupled travelling wavenumber k_x could be obtained iteratively using the dispersion equation for the coupled beam which is given in section 3.

$$D_b k_x^4 = m_b' \omega^2 - i\omega \tilde{Z}_p'. \tag{B.1}$$

where D_b is the bending stiffness of the beam, m_b' is mass per unit length of the beam, ω is frequency and $\tilde{Z}_p'$ is the approximate impedance of the plate. An initial value for k_x can be obtained if the semi-infinite width plate is assumed, and then the travelling trace wavenumber k_y of the finite plate can be obtained from the trace wavenumber relationship

$$k_y = \sqrt{k_p^2 - k_x^2} \tag{B.2}$$

where k_p is uncoupled wavenumber of the plate. Using the approximate plate impedance corresponding to this value of k_y an improved estimate for the wavenumber k_x is calculated and this procedure is repeated. At most frequencies the wavenumbers converge after a small number of iterations (for the present case a maximum of 19 iterations are used). Nevertheless, it has been discovered that erratic behaviour occurs when the coupled

wavenumber k_x does not converge during the iteration procedure. Figure B.1 and Figure B.2 illustrate this effect for the case of a damped plate. Figure B.1 shows the result after 18 iterations and Figure B.2 shows that after 19 iterations. For further iterations these results are repeated. Large differences can be seen around 18 Hz.

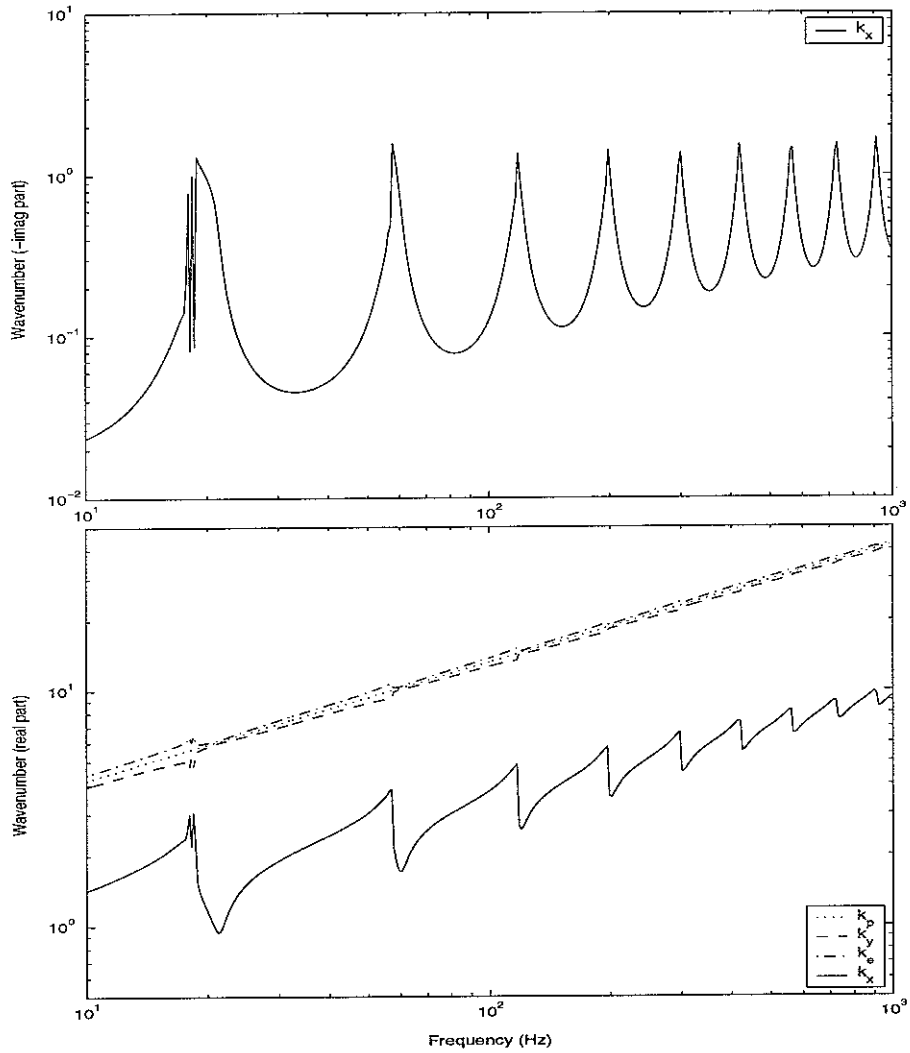

Figure B.1. Comparison of the wavenumber of the built-up structure consisting of an infinite beam and a finite width plate ($\eta_p = 0.05$ in the plate). 18 iterations.

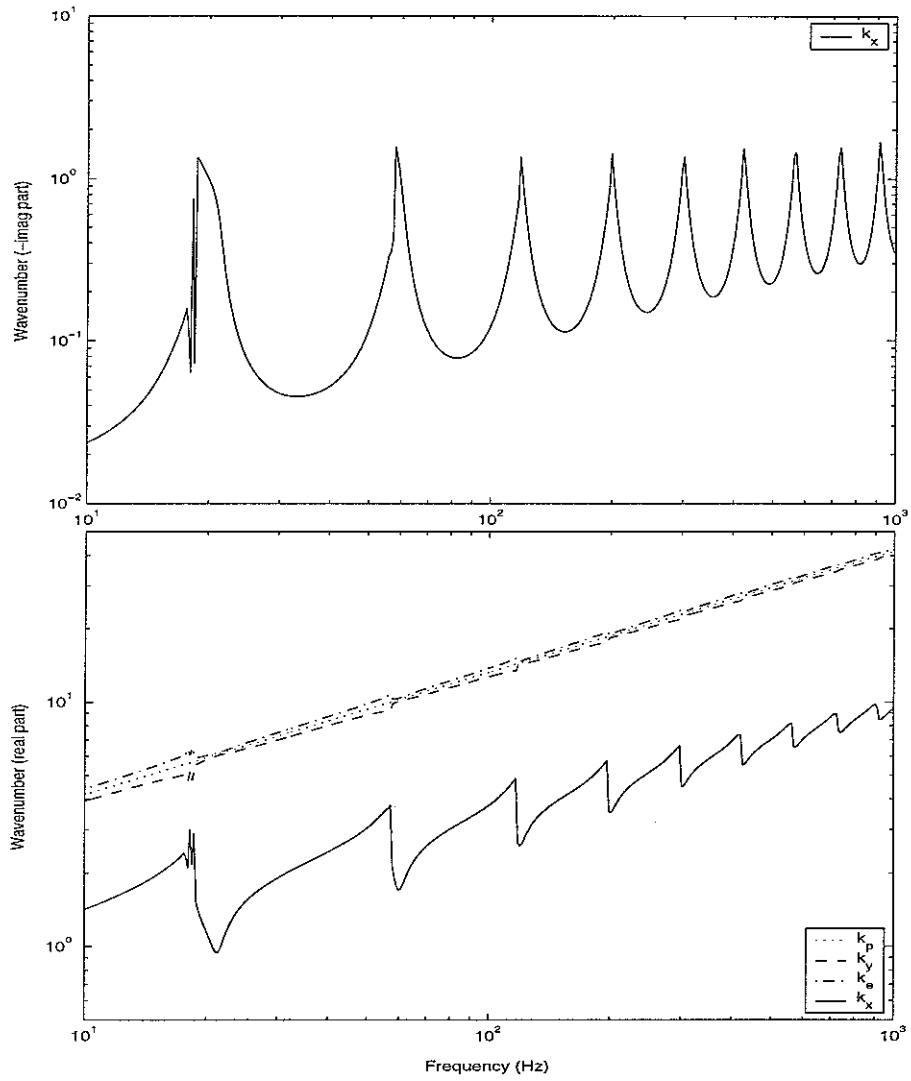

Figure B.2. Comparison of the wavenumber of the built-up structure consisting of the infinite beam and the finite width plate ($\eta_p = 0.05$ in the plate). 19 iterations.

In the figures above, k_p represents the free wavenumber of the plate, k_y the travelling wavenumber perpendicular to the beam, k_e the nearfield wavenumber of the plate in this direction and k_x the coupled wavenumber of the beam. It can be seen that at the first peak near 18.6 Hz the results do not converge during the iteration. This corresponds to the first anti-resonance of the plate. In this region it can be seen that k_y becomes smaller and both the real and imaginary parts of k_x become larger (Figure B.2). Because the wavenumbers

k_x and k_y are related through equation (B.2), the region in which the wavenumbers do not converge occurs when k_y, the wavenumber across the plate, becomes small and k_x, the corresponding travelling wavenumber along the beam becomes large. Therefore, it seems that the iterative method used is not appropriate for some frequency regions, normally near the peaks in the dispersion curves.

The solution to this problem can start from the dispersion equation (B.1). Because the attached plate impedance $\tilde{Z}'_p$ is a function of the wavenumber $\tilde{k}_x$ the equation can be rewritten as

$$f\left(\tilde{k}_x\right) = \tilde{D}_b \tilde{k}_x^4 - m'_b \omega^2 + i\omega\, \tilde{Z}'_p = 0 . \qquad \text{(B.3)}$$

As explained in section 3.3, it can be assumed that there are four roots close to the uncoupled beam wavenumber $\tilde{k}_b$ and normally two of them represent propagating waves and two nearfield waves. From the complex domain plot, these four roots can be identified. One example for this is shown in Figure B.3. Contours in the figure represent equal values of the function $\left|f\left(\tilde{k}_x\right)\right|$ given in equation (B.3) and the three circles in the figure represent roots where $\left|f\left(\tilde{k}_x\right)\right| = 0$. Comparing this figure with Figure B.2, it can be said that the root near $\mathrm{Re}(\tilde{k}_x) \approx 3.4$ is the correct value of the travelling wavenumber for the present case. A fourth root occurs near $\mathrm{Re}(\tilde{k}_x) \approx -3.4$.

Now, based on these complex domain contours and an appropriate numerical method, the wavenumber $\tilde{k}_x$ which does not converge can be obtained by calculating the root of this equation. Specifically to obtain such a complex root, Muller's method [7] can be a good approach. This method uses a quadratic equation which fits through three points in the vicinity of a root and the proper zero of the equation is used as the estimate of the root. This

process is repeated using the set of three points nearest the root being evaluated.

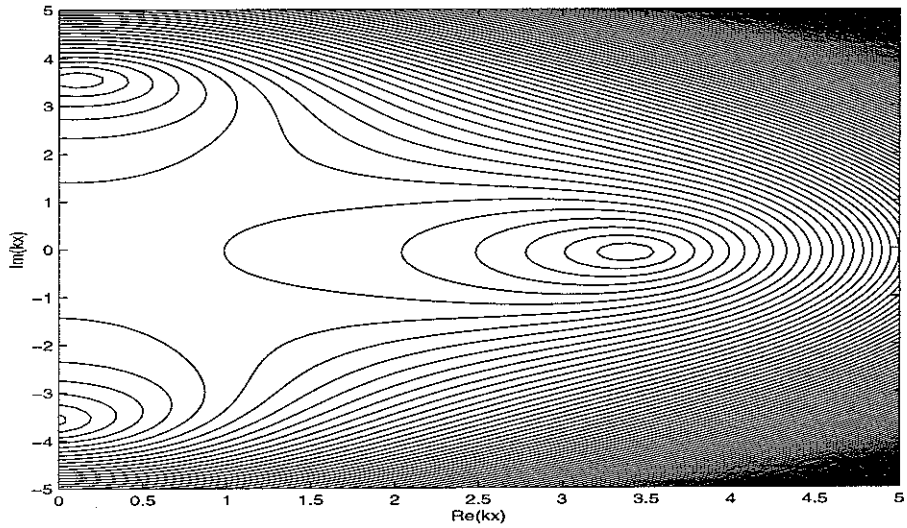

Figure B.3. Complex domain contours (right quadrants) and the roots at 90.6 Hz.

The first three initial values are selected at the complex domain contours such as Figure B.4, basically by trial and error. From the contours the root can be inferred approximately. For example, at 55.8 Hz near the second plate anti-resonance in Figure B.2, the root is expected to exist at the centre of the circles in the contours of Figure B.4. From Figure B.2, it can be inferred that the real part of $\tilde{k}_x$ is larger than 3 for this case and the root in the lower quadrant is expected to be the centre of circle near $\mathrm{Re}(\tilde{k}_x) \approx 3.6$ in Figure B.4. Another pole in the upper quadrant can be another wavenumber which is not appropriate for this case. Therefore, the three initial values are selected by trial and error near this circle. The arrows in Figure B.5 show the procedure converging to find the root near $\mathrm{Re}(\tilde{k}_x) \approx 3.6$ from initial values.

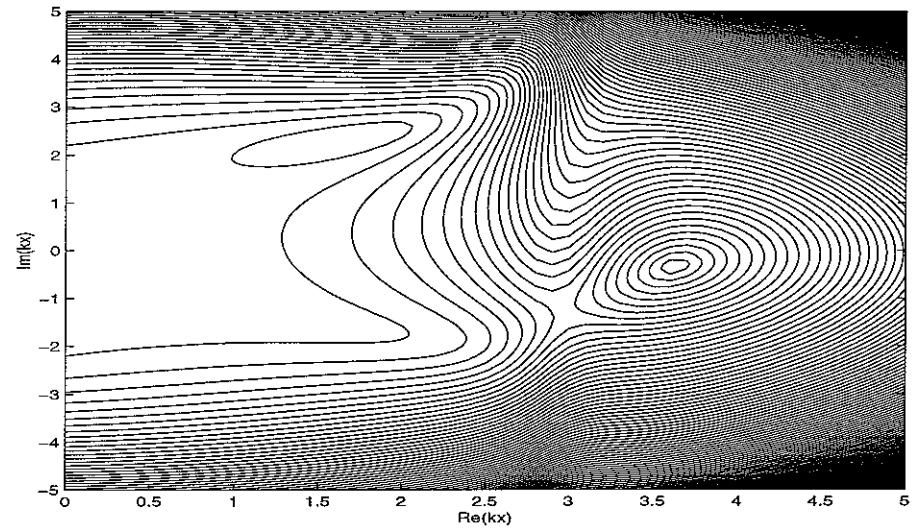

Figure B.4. Complex domain contours (right quadrants) and the roots at 55.8 Hz.

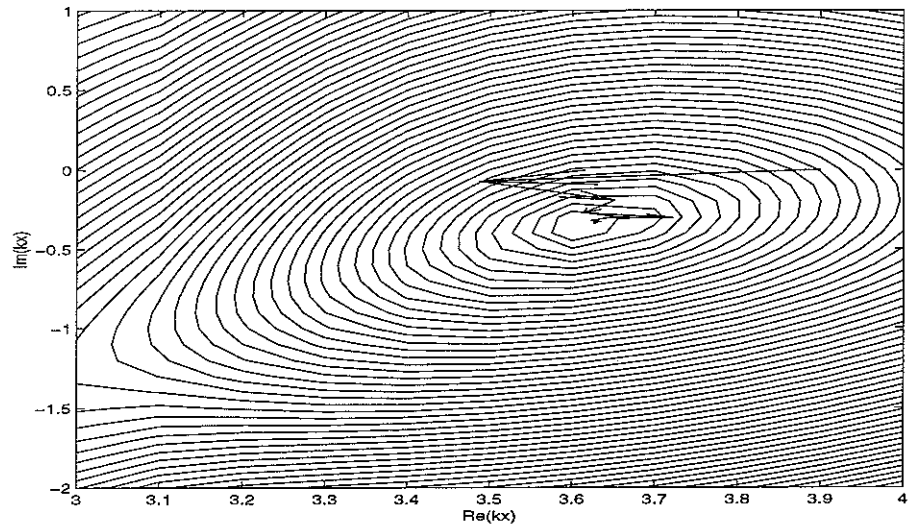

Figure B.5. Root-tracing calculated by Muller's method in the complex domain (55.8Hz).

As can be seen from Figures B.1 and B.2, during the iteration the frequency at which the wavenumber does not converge can be identified. If the calculated real part of the wavenumber shows more than 0.1 % difference between the results of the 18^{th} and 19^{th} iterations, then that wavenumber is regarded as a wavenumber which does not converge. The criterion 0.1 % was chosen by trial and error. For example, if 1 % is chosen then the number of calculations required using Muller's method can be reduced but results are not as good.

Conversely, if 0.01% is chosen then more calculation is necessary but the results show little improvement. On the basis of the 0.1 % criterion, 11 individual frequencies which do not converge are found and Muller's method is applied to obtain the exact root for the system. Newly calculated wavenumbers $\tilde{k}_x$ and the corresponding plate wavenumbers are shown in Figure B.6, from which it can be seen that the erratic behaviour has been eliminated. The approximate plate impedance, which depends on $\tilde{k}_x$, does not show any erratic fluctuation either, as seen in Figure B.7.

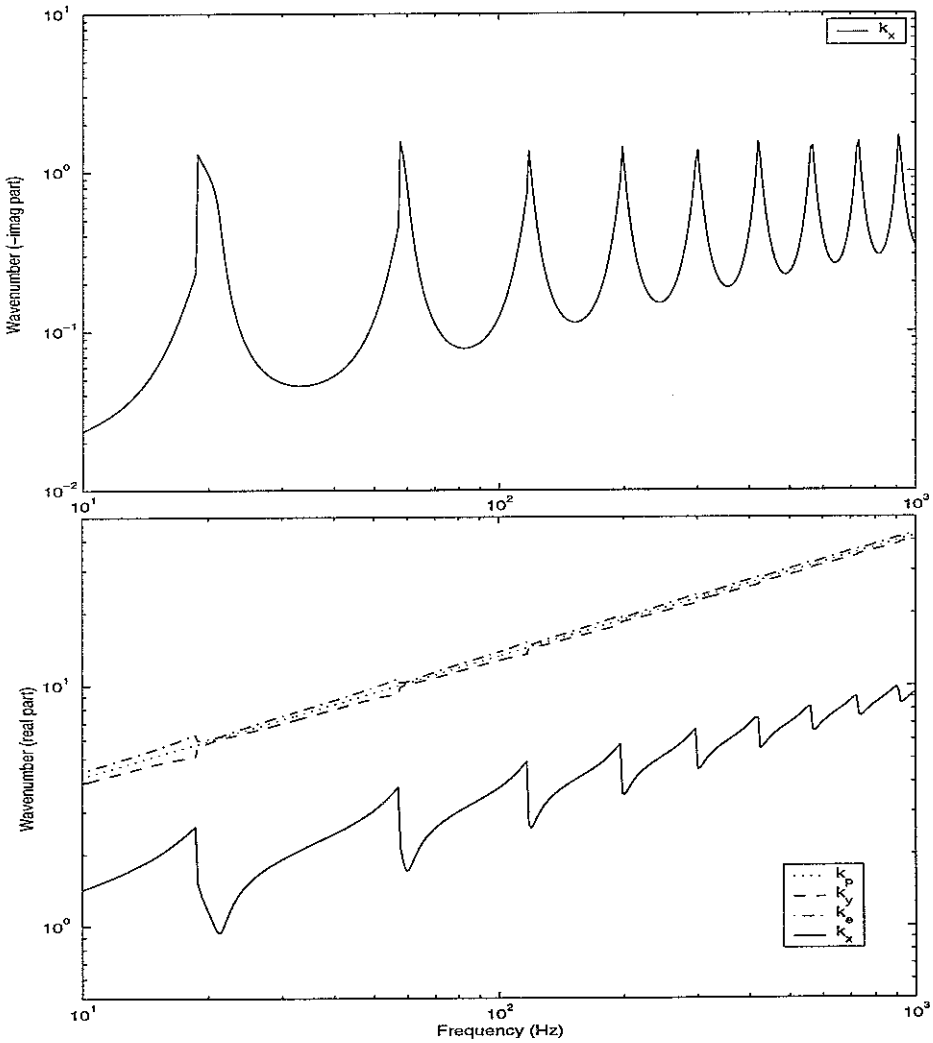

Figure B.6. Comparison of the travelling wavenumber k_x of the built-up structure as in Figure 2 ($\eta_p = 0.05$ in the plate) with the plate wavenumbers k_p, k_y, and k_e after using Muller's method.

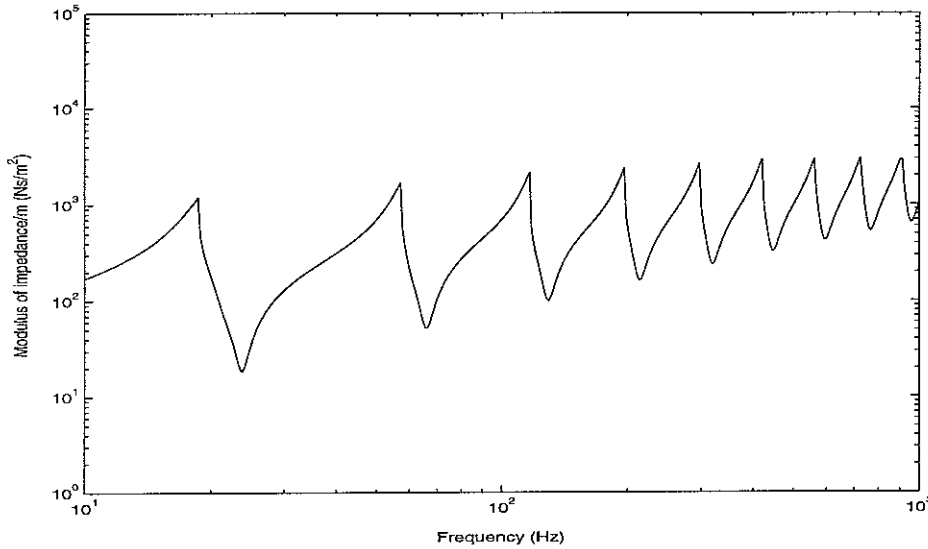

Figure B.7. Approximate impedance of the finite plate ($\eta_p = 0.05$ in the plate) after using Muller's method.